JGR Atmospheres

RESEARCH ARTICLE
10.1029/2023JD040078

Influence of the Neutralization Degree on the Ice Nucleation Ability of Ammoniated Sulfate Particles

Barbara Bertozzi[1,2], Robert Wagner[1], Kristina Höhler[1], Harald Saathoff[1], Ottmar Möhler[1], and Thomas Leisner[1]

[1]Institute of Meteorology and Climate Research, Karlsruhe Institute of Technology, Karlsruhe, Germany, [2]Now at Laboratory of Atmospheric Chemistry, Paul Scherrer Institute, Villigen, Switzerland

Abstract Previous laboratory measurements suggest that ammonium sulfate crystals (AS, $(NH_4)_2SO_4$) are efficient ice-nucleating particles under cirrus conditions. Sulfate particles not completely neutralized by ammonium are less well studied and include two other solids, ammonium bisulfate (AHS, NH_4HSO_4) and letovicite (LET, $(NH_4)_3H(SO_4)_2$). In this work, we have obtained the first comprehensive data set for the heterogeneous ice nucleation ability of crystallized particles in the AS–LET–AHS system as a function of their degree of neutralization at a temperature of about 220 K. Quantitative data on nucleation onsets, ice-active fractions, and ice nucleation active surface site densities were derived from expansion cooling experiments in a large cloud chamber and measurements with two continuous flow diffusion chambers. We found a strong dependence of the efficiency and the mode of heterogenous ice nucleation on the degree of neutralization. Ice formation for AS, mixed AS/LET, and LET crystals occurred by the deposition nucleation or pore condensation and freezing mode. The lowest nucleation onset was observed for AS, where 0.1% of the particles became ice-active at an ice saturation ratio of 1.25. This threshold gradually increased to 1.35 for LET, and abruptly further to 1.45 for mixed LET/AHS crystals, which partially deliquesced and induced ice formation via immersion freezing. Pure AHS crystals did not form due to the inhibition of efflorescence. Our data allow for a more sophisticated treatment of ice formation in the AS–LET–AHS system in future model simulations, which have so far only considered the available data for AS alone.

Plain Language Summary Sulfate particles that are partially or fully neutralized by ammonium are an important component of the atmospheric aerosol. The relative humidity in the environment determines whether they are present as aqueous solution droplets or as solid crystals. Depending on the degree of neutralization, three different crystalline solid phases can form: ammonium sulfate, $(NH_4)_2SO_4$, letovicite, $(NH_4)_3H(SO_4)_2$, and ammonium bisulfate, NH_4HSO_4. Knowledge of the phase state of the particles (i.e., aqueous or solid) is required because it affects a variety of important atmospheric processes, including light scattering, chemical reactions, and cirrus cloud formation. Cirrus ice crystals can form heterogeneously on solid particles and homogeneously in supercooled aqueous solution droplets. Heterogeneous ice formation by solid $(NH_4)_2SO_4$ particles has been well studied in the laboratory, while much less is known about the ice nucleation ability of the other two solids involved. We performed experiments in a large coolable cloud chamber at a temperature of about 220 K to derive a parameterization for the heterogeneous ice nucleation ability of particles in the $(NH_4)_2SO_4$–$(NH_4)_3H(SO_4)_2$–NH_4HSO_4 system as a function of their composition. This enables a differentiated treatment of this particle class in future model simulations of cirrus cloud formation.

Key Points:

- The heterogeneous ice nucleation ability of crystalline, ammoniated sulfate particles strongly depends on the degree of neutralization
- Ammonium sulfate, letovicite (LET), and their mixtures efficiently form ice by deposition nucleation or pore condensation and freezing at 220 K
- Mixtures of LET and ammonium bisulfate partially deliquesce and nucleate ice less efficiently by immersion freezing at 220 K

Supporting Information:

Supporting Information may be found in the online version of this article.

Correspondence to:

R. Wagner,
Robert.Wagner2@kit.edu

Citation:

Bertozzi, B., Wagner, R., Höhler, K., Saathoff, H., Möhler, O., & Leisner, T. (2024). Influence of the neutralization degree on the ice nucleation ability of ammoniated sulfate particles. *Journal of Geophysical Research: Atmospheres*, *129*, e2023JD040078. https://doi.org/10.1029/2023JD040078

Received 28 SEP 2023
Accepted 11 DEC 2023

Author Contributions:

Conceptualization: Barbara Bertozzi, Robert Wagner, Kristina Höhler, Harald Saathoff, Ottmar Möhler
Formal analysis: Barbara Bertozzi, Robert Wagner
Funding acquisition: Ottmar Möhler, Thomas Leisner
Investigation: Barbara Bertozzi, Robert Wagner, Harald Saathoff
Software: Barbara Bertozzi, Robert Wagner

1. Introduction

1.1. Heterogeneous Ice Nucleation by Crystalline Ammonium Sulfate

Crystalline ammonium sulfate (AS, $(NH_4)_2SO_4$) has been considered in model simulations as a potential candidate for ice-nucleating particles (INPs) under cirrus conditions (Abbatt et al., 2006; Beer et al., 2022; Bhattacharjee et al., 2010; Jensen et al., 2018; Penner et al., 2018). Such INPs can initiate ice formation at supersaturations lower than those required for the homogeneous freezing of aqueous solution droplets (Vali et al., 2015), thereby affecting the microphysical properties of cirrus and its effect on climate (Kärcher et al., 2022; Maloney et al., 2022). The inclusion of AS in cloud models along with other INP types such as mineral dust, soot, and glassy organics is supported by a number of laboratory studies showing that the onset of nucleation for heterogeneous ice formation on crystalline AS is below an ice saturation ratio (S_{ice}) of 1.3 at temperatures <230 K (Abbatt et al., 2006;

Supervision: Robert Wagner
Visualization: Barbara Bertozzi, Robert Wagner
Writing – original draft: Robert Wagner
Writing – review & editing: Barbara Bertozzi, Robert Wagner, Kristina Höhler, Harald Saathoff, Ottmar Möhler

Baustian et al., 2010; Hoose & Möhler, 2012; Ladino et al., 2014; Shilling et al., 2006; Wise et al., 2009). Threshold values of S_{ice} = 1.20 and 1.25, for example, were used in models for the heterogeneous AS freezing mode (Beer et al., 2022; Penner et al., 2018), while homogeneous freezing starts in the range of $S_{ice} \approx$ 1.5–1.7 for temperatures between 230 and 185 K (Koop et al., 2000), with one recent study even pointing to S_{ice} values as high as 2 at the lowest temperatures (Schneider et al., 2021). The model simulations need to incorporate the hysteresis effect in the hygroscopic behavior to accurately predict the phase state of AS (i.e., either liquid or crystalline), as the efflorescence relative humidity (ERH, 37% at 298 K) is lower than the deliquescence relative humidity (DRH, 80% at 298 K) (Tang & Munkelwitz, 1994). For humidities between ERH and DRH, the phase state of AS therefore depends not only on the instantaneous relative humidity (RH), but also on the RH history of the air parcel. Efflorescence is the first requirement for AS to act as an INP, and model simulations indeed indicate widespread regions with high solid fractions, for example, in the upper troposphere of the Northern Hemisphere (Beer et al., 2022; Colberg et al., 2003; J. Wang et al., 2008). The formation of solid particles could be aided by a process known as contact efflorescence, where, for example, a mineral dust particle collides with an AS solution droplet and causes its crystallization at a higher RH compared to the homogeneous ERH (Davis et al., 2015; Kirpes et al., 2022; Ushijima et al., 2018). A second mechanism for heterogeneous efflorescence is the immersion mode, in which a solid particle acts as a crystallization nucleus from within the AS solution droplet (Han & Martin, 1999). After efflorescence, the second requirement for heterogeneous ice formation by AS is that the onset of ice formation occurs before the DRH is exceeded and the salt crystals transform into aqueous solution droplets (Braban et al., 2001). The above-mentioned laboratory studies underline that this competition between heterogeneous ice formation on the one hand and deliquescence with subsequent homogeneous freezing on the other hand is indeed in favor of heterogeneous ice formation at sufficiently low temperatures, that is, in the cirrus range.

There are two important aspects that complicate the comparatively simple observations discussed above to describe the ice nucleation behavior of pure AS. Firstly, a significant fraction of AS particles in the atmosphere could be internally mixed with organic matter (Froyd et al., 2009; Martinsson et al., 2019). This can have a variety of consequences depending on the amount and viscosity of the organic material (Schill & Tolbert, 2013). With regard to the crystallization behavior, previous experimental findings range from a minor influence on the efflorescence properties to the complete suppression of efflorescence at sufficiently low temperature and/or high organic mass fraction (Bodsworth et al., 2010; Wise et al., 2010; Xu et al., 2022). AS crystals entrapped in a less viscous organic solution can act as immersion freezing nuclei with ice nucleation onsets in the range of S_{ice} = 1.35–1.40, which is approximately midway between the ice nucleation thresholds of pure crystalline AS and pure organics (Ladino et al., 2014; Schill et al., 2014). Small mass fractions of highly viscous secondary organic matter condensing on crystalline AS particles at $T \leq 228$ K rapidly shield the ice nucleation capability of the AS core and shift the onset of ice nucleation to values $S_{ice} \geq 1.45$ (Bertozzi et al., 2021). The ice nucleation threshold of such deactivated, uniformly coated AS crystals decreases again to $S_{ice} \approx 1.35$ after ice cloud processing, presumably due to a redistribution of the organic coating material or a transformation of the structure of the coating from compact to porous (Adler et al., 2013).

As for the second aspect mentioned above, we disregard the mixing with organic matter but consider that ammoniated sulfate particles do not necessarily have to be completely neutralized to AS. Depending on the temporal and spatial distribution of ammonia sources and the efficiency with which ammonia is transported through the atmosphere, the aerosol composition can change significantly with altitude and between remote and polluted regions (Nault et al., 2021). We define the degree of neutralization x of sulfate particles by ammonium as the ratio between the moles of NH_4^+ and the sum of the moles of NH_4^+ and H^+. x ranges from 0 for sulfuric acid solutions droplets to 1 for AS. If neutralization is incomplete, two other crystalline solid phases can form, namely ammonium bisulfate (AHS, NH_4HSO_4, $x = 0.5$) and letovicite (LET, $(NH_4)_3H(SO_4)_2$, $x = 0.75$). Previous model simulations on the global distribution of solid and liquid particles in the AS–LET–AHS system disagree on which solid form is predominant (Colberg et al., 2003; J. Wang et al., 2008). While Colberg et al. (2003) found LET to be the most abundant solid, the simulations of J. Wang et al. (2008) showed higher neutralization, with >90% of the solid mass fraction consisting of AS. An important parameter controlling the degree of neutralization in the model simulations, especially for aerosol particles in the upper troposphere, is the retention efficiency of ammonia (NH_3) during the freezing of cloud droplets to ice crystals. A low retention efficiency allows NH_3 dissolved in liquid cloud droplets to be released into the upper troposphere upon freezing during deep convection (Ge et al., 2018), resulting in highly neutralized particles as, for example, observed in the tropical tropopause layer

(Froyd et al., 2009). Recently, chemical transport models (CTMs) were compared against a comprehensive set of aircraft observations of aerosol composition with broad spatial coverage around the globe (Nault et al., 2021). The models frequently overestimated the degree of neutralization of sulfate aerosol particles observed in the measurements, for example, did not reproduce regions of lower x values in the upper troposphere over Canada and US. As will be discussed in Section 1.3, heterogeneous ice nucleation measurements for particles with $x < 1$ are very rare, which means that there is as yet no solid data basis for quantitatively describing the heterogeneous ice nucleation behavior of sulfate particles that are not fully ammoniated. Before we address this point, which is the focus of this work, we have to take a closer look at what is known about the crystallization behavior of such partially neutralized particles, since efflorescence is a prerequisite for them to act as INPs.

1.2. Crystallization Pathways in the AS–LET–AHS System and Potential Ice Nucleation Behavior

The crystallization pathways in the AS–LET–AHS system have been extensively studied in the laboratory (Colberg et al., 2003, 2004; Cziczo & Abbatt, 2000; Martin et al., 2003; Mifflin et al., 2009; Rosenoern et al., 2008; Schlenker & Martin, 2005; Schlenker et al., 2004; Spann & Richardson, 1985; Tabazadeh & Toon, 1998; Tang & Munkelwitz, 1994). The study by Schlenker and Martin (2005), which is also one of the most comprehensive, has great relevance for the experimental procedure used in this work and will therefore be described in more detail. In Schlenker and Martin (2005), initially liquid ammoniated sulfate particles with x between 0.5 and 1 were exposed at 293 K to a fixed sequence of RH values in the order of 60%, followed by 3%, followed by 30%. After exposure to this RH program, infrared extinction spectra were recorded to determine the phase state of the particles and which solid had formed. The final conditioning step at 30% RH took advantage of the hysteresis effect to determine whether crystallization had taken place at 3% RH. For particles that had completely crystallized at 3% RH, no liquid water uptake would be expected at 30% RH, as this value is below the initial DRH for all solids involved and their mixtures (Clegg et al., 1998; Tang & Munkelwitz, 1994). For $x = 0.50$ and 0.55, the infrared spectra recorded after the RH program showed completely aqueous particles, indicating the inhibition of efflorescence, which was similarly observed in an aerosol flow tube study with submicron AHS solution droplets at temperatures down to 238 K (Cziczo & Abbatt, 2000). In contrast, Colberg et al. (2003) detected the crystallization of LET in levitated AHS solution droplets at 15%–16% RH between 270 and 260 K. For $x = 0.60$, 0.65, and 0.70, the particles were dominantly crystalline after exposure to the RH program and formed a mixture of AHS and LET (Schlenker & Martin, 2005). It is likely that LET precipitated first and triggered the crystallization of AHS heterogeneously. Small residual amounts of liquid water (<5% by mass) were considered to be most likely due to aqueous pockets trapped in the larger particles of the aerosol size distribution. For $x > 0.7$, such aqueous pockets were no longer observed and the RH processed particles were completely crystalline. For $x = 0.75$, Schlenker and Martin (2005) indicated the formation of pure LET particles, but a follow-up study showed that an externally mixed particle population was formed instead, consisting of LET on the one hand and internally mixed particles of AHS and AS on the other (Rosenoern et al., 2008). Repeated hydration—dehydration cycles increased the LET fraction, but some internally mixed AHS/AS particles remained even after multiple cycles. For compositions in the range from $x = 0.80$ to $x = 0.95$, internally mixed particles of LET and AS were formed, and finally pure AS for $x = 1$ (Schlenker & Martin, 2005).

What would be the general ice nucleation behavior of the particles after going through the RH program of Schlenker and Martin (2005)? For $x = 0.50$ and 0.55, homogeneous freezing will be the only feasible ice nucleation pathway if crystallization is inhibited. In the range from $x = 0.75$ to $x = 1$, if we disregard the small proportion of internally mixed AHS/AS particles at $x = 0.75$ for the time being, we must consider either pure LET and AS or mixtures of the two. LET has a relatively high DRH of about 70% at 298 K (Spann & Richardson, 1985; Tang & Munkelwitz, 1994), increasing to about 73% at 263 K (Colberg et al., 2003). Assuming that there is a further increase in the DRH of LET towards cirrus temperatures, this may lead to a situation similar to AS, that is, heterogeneous ice nucleation could occur before the deliquescence point of the LET crystals is surpassed. The relevant question regarding the ice nucleation behavior would then be whether there are differences in the efficiency of ice formation on the different crystal types, that is, LET, LET/AS, and AS. The underlying mode of ice nucleation could be either deposition nucleation or pore condensation and freezing (PCF) (Marcolli, 2014; Vali et al., 2015). We are not aware of any study and we cannot distinguish in our current experiments which of these two ice nucleation modes is active.

The hygroscopic behavior of mixed AHS/LET particles in the range from $x = 0.60$ to $x = 0.70$ is more complex and was first studied by Spann and Richardson (1985). They found that the onset of the dissolution of the solid particles occurred at about 39% RH at 298 K, that is, near the deliquescence point of AHS (Tang & Munkelwitz, 1994). At this threshold, the AHS fraction of the mixed AHS/LET crystals dissolves completely, while the LET fraction

remains as a solid core. Measurements of the deliquescence onset at low temperatures have not yet been reported. If the onset DRH of the AHS fraction does not increase significantly with decreasing temperature, the mixed AHS/LET particles could also begin to dissolve under cirrus conditions before reaching the RH region where the air is supersaturated with respect to ice. This would leave immersion freezing by the solid LET core as the only possible pathway for heterogeneous ice formation. However, as the humidity continues to increase, the embedded solid core continuously shrinks according to the lever rule of the phase diagram and eventually dissolves completely. The dissolution of the LET core may be enhanced if it is not present as a single, compact crystalline core, but as smaller fragments with increased solubility (Rosenoern et al., 2008). On the contrary, subpopulations of mixed AHS/LET particles were observed to have a delayed onset of deliquescence >39% RH at room temperature (Mifflin et al., 2009). This could be due to a special particle morphology where the AHS part is surrounded by a thick LET layer that slows down water uptake. In such a situation, a mixed AHS/LET particle might also be prone to deposition mode ice nucleation/PCF by the LET layer, which underlines that besides the net composition of a particle, its morphology could also have a crucial influence on the pathway of ice formation. Similar considerations as for AHS/LET also apply to the small proportion of AHS/AS particles that form during crystallization for $x = 0.75$.

1.3. Previous Ice Nucleation Measurements in the AS–LET–AHS System and Aim of This Work

The considerations from the previous section suggest that different ice nucleation modes may be active for ammoniated sulfate particles in the composition range from $x = 0.5$ to $x = 1$, namely homogeneous freezing, immersion freezing, and deposition nucleation/PCF. Apart from the two limiting cases, (a), the homogeneous freezing of AHS solution droplets, which are difficult to crystallize (Cziczo & Abbatt, 2001; Koop et al., 1999), and (b), the heterogeneous ice nucleation measurements with crystalline AS mentioned above, there are few data on ice nucleation for intermediate neutralization degrees (Chen et al., 2000; Zuberi et al., 2001). Zuberi et al. (2001) performed thermal cycling experiments (in the range between room temperature and 183 K) with initially aqueous AS and AHS solution droplets to generate mixed-phase particles that contained a solid core of either AS or LET immersed in the solution, and their ice nucleation behavior was subsequently studied. For AS, the morphology of the immersed solid could be controlled to have either numerous microcrystals or only one or two larger crystals. In the case of microcrystals, efficient heterogeneous ice formation by immersion freezing was observed at S_{ice} close to 1. In contrast, the onset of ice nucleation was shifted to near the homogeneous freezing threshold when the solid was in the form of one or two larger crystals. The solid LET inclusions were always in the form of larger crystals, and the ice nucleation onset was close to homogeneous freezing conditions. For temperatures between 233 and 213 K, Chen et al. (2000) reported freezing onsets at 95%–100% RH for AHS particles that were presumably at least partially crystallized and contained solid LET within an acidified bisulfate solution.

The objective of this work is to establish a comprehensive data set for the ice nucleation behavior of crystalline, ammoniated sulfate particles in the composition range from $x = 0.5$ to $x = 1$ at cirrus temperatures. In a first set of experiments, we mimicked the RH processing from Schlenker and Martin (2005) and combined it with measurements of the particles' ice nucleation behavior under cirrus conditions. Here, we first generated aqueous solution droplets of a certain composition x and dried them at room temperature to RH $\leq$ 3%. For the final conditioning step at intermediate RH, we injected the dried particles into the aerosol and cloud chamber AIDA (Aerosol Interaction and Dynamics in the Atmosphere) held at 223 K and 31%–38% RH. Infrared extinction as well as light-scattering depolarization measurements were used to infer whether or not crystallization has occurred. The ice nucleation ability of the processed particles was investigated both in situ, by performing expansion cooling experiments in the AIDA chamber, and ex situ, by sampling the particles and probing them with two continuous flow diffusion chambers (CFDCs). In a second procedure, we obtained ice nucleation data for all compositions in a single experiment. Here, we first injected aqueous sulfuric acid solution droplets with $x = 0$ into the AIDA chamber and then added a continuous flow of ammonia to gradually neutralize the particles. Simultaneously, we measured the composition-dependent ice nucleation ability of the particles with the CFDCs. In addition to the ice nucleation data, our experiments provide new information on the hygroscopic behavior of particles in the AS–LET–AHS system at low temperatures.

2. Methods

2.1. General Setup and Experimental Procedure

This work uses a setup and instrumentation described in detail in a recent article on ice nucleation experiments with crystalline ammonium nitrate (Wagner et al., 2020). We provide a brief summary here. All experiments were

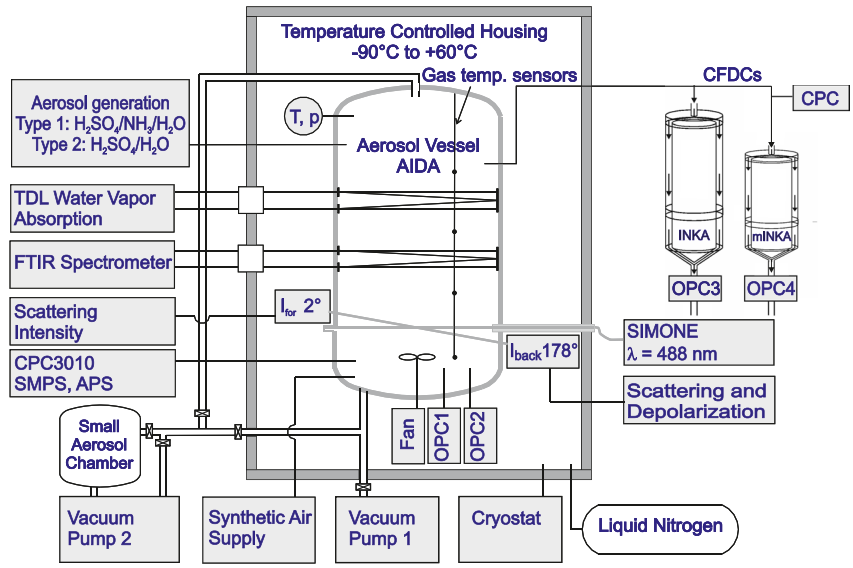

Figure 1. Schematic of the instrumentation of the Aerosol Interaction and Dynamics in the Atmosphere aerosol and cloud chamber facility including the two continuous flow diffusion chambers used for ex situ ice nucleation measurements. All abbreviations are explained in Section 2.

conducted in the 84 m^3 aerosol and cloud simulation chamber AIDA at the Karlsruhe Institute of Technology (Figure 1). The aerosol vessel is located in a large thermostated housing, the temperature of which was controlled to 223 K for the present experiments. A vertical array of thermocouples was used to measure the mean gas temperature in the chamber. The cleaned and evacuated AIDA vessel (<1 hPa) was first conditioned to the desired relative humidity by evaporating an appropriate amount of ultrapure water into the chamber, and then filled to ambient pressure with dry, particle-free synthetic air. The water vapor partial pressure, p_w, was measured in situ by a tunable diode laser (TDL) absorption spectrometer with an accuracy of ±5% (Fahey et al., 2014). Tabulated expressions for the temperature-dependent saturation water vapor pressure over ice and supercooled liquid water were used to compute S_{ice} and RH (saturation ratio with respect to liquid water, S_{liq}, expressed as a percentage) from p_w (Murphy & Koop, 2005). After refilling to ambient pressure, a mixing fan located about 1 m above the bottom of the chamber was started to ensure efficient mixing for the subsequent experiments.

As mentioned in the introduction, two types of experiments were conducted. For the first type, we prepared AS–LET–AHS bulk solutions in the composition range from $x = 0.5$ to $x = 1$ by dissolving appropriate amounts of AHS (Merck, 99.8%) and AS (Merck, ≥99.5%) in ultrapure water. The overall solute concentration was 8 g/100 mL. A total of eight experiments of this type were carried out with x = 0.5, 0.55, 0.6, 0.675, 0.75, 0.8, 0.9, and 1. To simulate the RH processing by Schlenker and Martin (2005), we first generated aqueous solution droplets by aerosolizing the bulk solutions with an ultrasonic nebulizer (GA 2400, SinapTec) and then dried the aerosol flow to typically RH ≤ 3% with two silica gel diffusion dryers (Topas GmbH) connected in series. The dried particles were then injected into the AIDA chamber at 223 K and 31%–38% RH, which thus represented the final conditioning step at medium relative humidity. The number concentration of injected aerosol particles was usually about 1,000 cm^{-3}, measured with a condensation particle counter (CPC, model 3010, TSI). Aerosol size distributions were measured with a combination of a scanning mobility particle sizer (SMPS, model 3071A, TSI) and an aerodynamic particle spectrometer (APS, model 3321, TSI). The measured mobility and aerodynamic diameters were merged into a common size scale, that is, the equal-volume sphere diameter, by employing a dynamic shape factor of 1.1 and a particle density of 1.78 g cm^{-3}. Due to the same solute concentration, the particle size spectra were very similar in all experiments and closely corresponded to the shape of a unimodal lognormal distribution with the center at about 0.9 μm and a mode width of about 1.2.

The composition and phase of the aerosol particles inside the AIDA chamber were derived from two types of in situ instruments. Similar to Schlenker and Martin (2005), we used infrared spectroscopy and recorded infrared extinction spectra of the aerosol particles with a FTIR spectrometer (Fourier Transform Infrared, model IFS 66v, Bruker) coupled to an internal multiple reflection cell set to an optical path length of 166.8 m (Wagner

et al., 2006). In addition, we measured the near-backscattering (178° scattering angle) linear depolarization ratio of the aerosol particles at a wavelength of 488 nm with the instrument SIMONE (German abbreviation for "Scattering intensity measurements for the optical detection of ice") (Schnaiter et al., 2012). As in previous experiments with sea salt aerosol (SSA) particles of similar size that were present in three different phases, that is, completely liquid, completely crystalline, or mixed solid-liquid, different depolarization ratios can be assigned to different phase states, that is, zero for homogeneous aqueous particles, high values (>10%) for completely crystalline particles, and small non-zero percentage values for aqueous particles with a solid core (Wagner et al., 2018). As detailed in Section 2.2, the ice nucleation ability of the ammoniated sulfate particles in each of the experiments of the first type was measured with the two CFDCs at 221 and 217 K and with an expansion cooling run in the AIDA chamber.

In the second type of experiment, we started by injecting aqueous sulfuric acid solution droplets ($x = 0$) into the AIDA chamber at 223 K and 25% RH. The droplets were produced by passing synthetic air over a small amount of concentrated sulfuric acid contained in a heated glass tube (413 K) and were about 0.9 μm in diameter (Schneider et al., 2021). Then we switched on a continuous flow of 2–4 SCCM ammonia (2% NH_3 in air) to gradually neutralize the H_2SO_4/H_2O solution droplets over a time period of 5–6 hr. The change in droplet composition, the eventual crystallization of the droplets, and the further compositional change in the solid phase were again monitored by infrared spectroscopy and depolarization measurements. At the same time, the ice nucleation ability of the transforming particles was continuously measured with the two CFDCs, one operated at 221 K and the other at 217 K (Section 2.2). Further details are given in Sections 3.2 and 3.3, where we will also explain in more detail the explicit motivation for conducting this continuous in situ neutralization experiment in addition to the experiments of the first type with fixed particle composition.

2.2. Ice Nucleation Measurements

The ice nucleation measurements in the AIDA chamber simulate the ascent of moist air in the atmosphere through an expansion cooling experiment in which the chamber pressure is reduced by powerful vacuum pumps located in the basement of the AIDA facility (Figure 1), resulting in a decrease in gas temperature and an increase in relative humidity. Ice crystals that started to nucleate at a critical S_{ice} threshold were quantitatively counted with two optical particle counters (OPC1 and OPC2, model welas 2300 and 2500, Palas) mounted in the free space between the bottom of the cloud chamber and the floor of the thermostated housing. The ice particle number concentration was normalized to the number of aerosol particles present at the time of nucleation to determine the ice-active fraction of the aerosol population, f_{ice}. By dividing f_{ice} by the aerosol surface area per particle, we calculated the ice nucleation active surface site density, n_s, with an estimated overall uncertainty of ±40% (Ullrich et al., 2017). n_s is a function of both ice saturation ratio and temperature and indicates the cumulative number of nucleation sites per surface area that have become ice active up to the specified values for S_{ice} and T (Connolly et al., 2009). Analysis in terms of n_s is a convenient method for normalizing ice nucleation data for the same aerosol type when different particle sizes have been used in the experiments, or for comparing the ice nucleation efficiency of different aerosol types. It thus offers an easy-to-implement aerosol-specific parameterization for cloud models (Hoose & Möhler, 2012).

In addition to the expansion experiments, f_{ice} and n_s data were derived from measurements with two CFDCs sampling the aerosol particles suspended in the AIDA chamber. The first was a stationary instrument permanently installed at the AIDA facility, called INKA (Ice Nucleation Chamber of the Karlsruhe Institute of Technology) (DeMott et al., 2018; Schiebel, 2017; Wagner et al., 2020). The second was a mobile version of INKA, called mINKA, which was developed for experiments in the Cosmics Leaving Outdoor Droplets (CLOUD) chamber at CERN (Bertozzi, 2021; M. Wang et al., 2022), but was also available for this study. Both INKA and mINKA are CFDCs with vertical cylindrical geometry (Rogers, 1988). The cylinder walls of INKA have a length of 150 cm, with the upper two-thirds (~100 cm) designated as the diffusion section, where the aerosol particles are exposed to a defined ice supersaturation, and the lower third (~50 cm) as the evaporation section, where S_{ice} is controlled to the value 1. The term "evaporation section" refers to ice nucleation experiments performed under mixed-phase cloud conditions, which means that supercooled cloud droplets evaporate in this section due to sub-saturated conditions relative to liquid water, so that co-existing ice crystals can be selectively counted. With respect to our measurements presented here under cirrus conditions, in which only ice crystals are formed, the evaporation section can simply be regarded as an inert segment in which neither new ice crystals are formed nor existing ones

continue to grow. mINKA has shorter cylinder walls (85 cm) than INKA, but is operated without an evaporation section to maximize the residence time of the particles in the diffusion section where nucleation and growth of the ice crystals can take place. Further technical details and a thorough comparison of the performance of the two CFDCs for different types of aerosol particles are given in Bertozzi (2021). Both instruments were operated in the "humidity scan mode," where the temperature experienced by the aerosol particles was kept constant and RH was increased from ice-saturated to water-saturated conditions at an average dS_{ice}/dt rate of about 0.03 min^{-1}. During the experiments of the first type with fixed particle composition, humidity scans were performed with both INKA and mINKA for two temperatures of 221 and 217 K. For the in situ neutralization experiment, INKA was set at 217 K and mINKA at 221 K, and the ice nucleation ability of the particles was measured continuously every 30 min. In the same way as described above for the AIDA measurements, f_{ice} and n_s were computed from the number concentration of nucleated ice crystals measured with OPCs connected to the outlet of the CFDCs (OPC3 and OPC4, customized CI-3100, Climet).

3. Results and Discussion

We will present and discuss our measurement data in the following order. In Section 3.1, we describe the general ice nucleation behavior in the AS–LET–AHS system as revealed by the experiments with fixed particle composition. We focus here on the AIDA data because they provide additional information about the phase state and hygroscopic behavior of the particles based on the infrared and depolarization measurements. In Section 3.2, we then show a quantitative comparison of the ice nucleation efficiencies measured in AIDA and with the two CFDCs INKA and mINKA. We also develop questions to be answered by the additional in situ neutralization experiment, which is then discussed in Section 3.3. In Section 3.4, we provide our best estimates for the n_s values as a function of particle composition and ice saturation ratio, which is useful for future model calculations. Further results of our work, that is, the deliquescence properties of the investigated particles at low temperatures, are briefly summarized in Section 3.5.

3.1. General Overview of the Composition-Dependent Ice Nucleation Behavior in the AS–LET–AHS System

3.1.1. Infrared Extinction Spectra of the AS–LET–AHS Particles After the RH Processing

We start our discussion with a brief look at the infrared extinction spectra of the AS–LET–AHS particles after the RH processing, that is, after droplet generation, drying, and injection into the AIDA chamber at 31%–38% RH and 223 K (Figure 2), as this allows a direct comparison with the results of Schlenker and Martin (2005). We observed the signature of liquid water as a shoulder at 3,450 cm^{-1} in only two spectra, namely for $x = 0.5$ and $x = 0.55$. For $x = 0.5$, we assume that the entire particle population was in the liquid phase, which means that none of the pure AHS solution droplets crystallized. This assumption is confirmed by the observations of the depolarization ratio of the particles and their hygroscopic and ice nucleation behavior, which are discussed in the following sections. Liquid water was also observed for $x = 0.55$, but the shoulder at 3,450 cm^{-1} was less pronounced than at $x = 0.5$. Further analysis, presented below, revealed that an external mixture of particles was formed, consisting of approximately 35% liquid droplets and 65% crystallized AHS/LET particles. This differs from the experiments of Schlenker and Martin (2005), where completely aqueous particles were observed for this composition. For $x \geq 0.6$, no macroscopic liquid water extinction signature was detectable in the FTIR spectra anymore, indicating that the particles were dominantly crystalline. Note that this does not rule out the possibility of a very small, undetectable amount of trapped aqueous pockets, even for $x = 1$. We have previously confirmed the presence of such aqueous pockets in pre-activation experiments with dried AS crystals (Wagner et al., 2014). The crystals were cooled to 195 K where aqueous AS pockets could freeze homogeneously, and then reheated to temperatures just below the eutectic melting of ice and AS at 254 K. Due to the entrapped ice pockets, the temperature-processed AS crystals became ice-active at temperatures between 244 and 251 K, that is, under conditions where unprocessed AS particles lack intrinsic heterogeneous ice nucleation ability.

To conclude this short section, we refer to a look-up table that summarizes the crystallization behavior as well as the later observed ice nucleation mode and onset condition for the experiments with fixed particle composition (Table 1). The content of Table 1 is based on the observations described in this and the following two Sections 3.1.2 and 3.1.3.

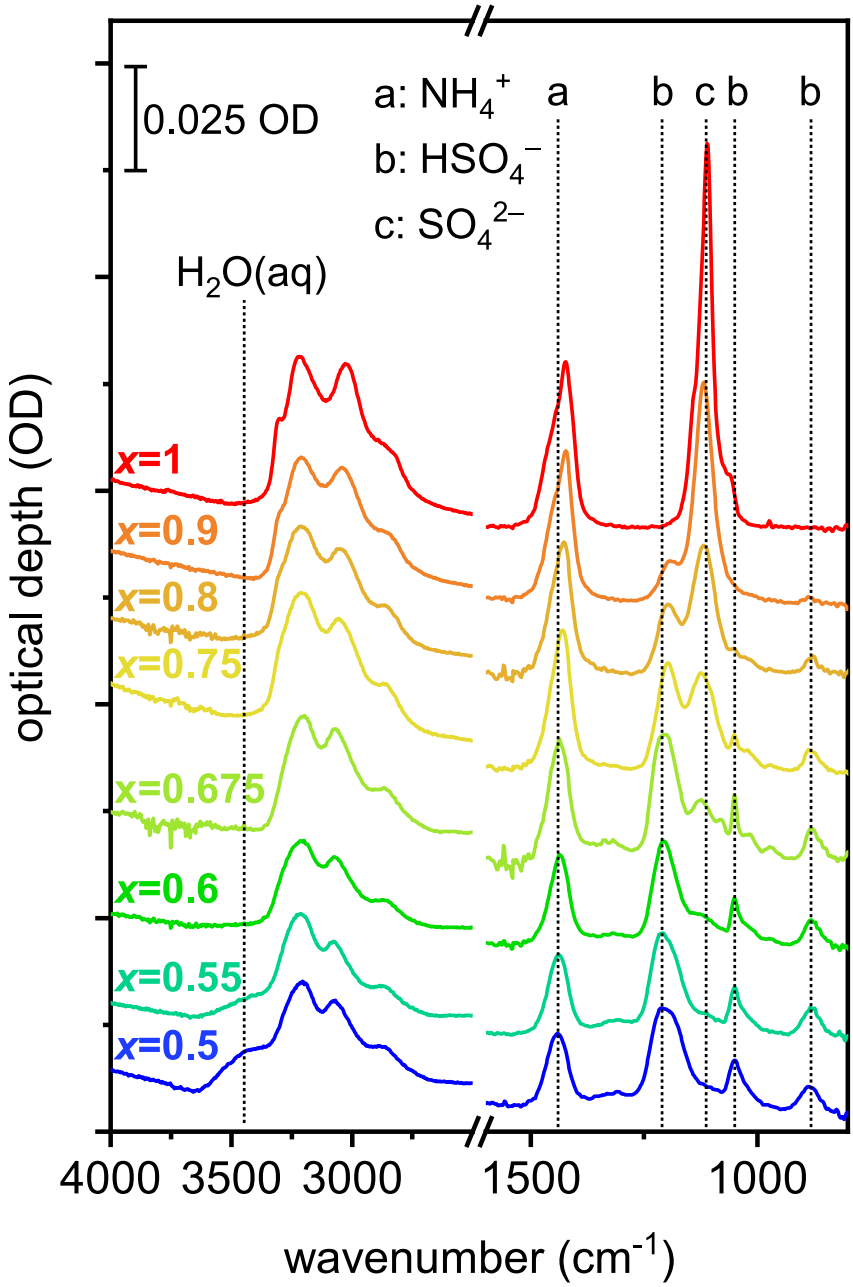

Figure 2. Infrared extinction spectra of ammoniated sulfate particles first nebulized from AS–LET–AHS bulk solutions of given neutralization degree x, dried at 298 K to RH of typically ≤3%, and then injected into the Aerosol Interaction and Dynamics in the Atmosphere chamber at 223 K and 31%–38% RH. The dotted lines labeled (a), (b), and (c) in the wavenumber region from 1,600 to 800 cm^{-1} show the assignment of the extinction bands to the NH_4^+, HSO_4^-, and SO_4^{2-} ions, respectively (Schlenker & Martin, 2005). A prominent shoulder, which becomes visible if liquid water is present, is located at about 3,450 cm^{-1}. The displayed spectra are offset for clarity and have been corrected for imbalances in the gas phase H_2O and CO_2 concentrations between the reference runs before aerosol injection and the later sample runs.

3.1.2. Ice Nucleation Behavior of Particles in the AS–LET–AHS System With $x = 0.5$ and $x = 1$

As for the ice nucleation experiments carried out in this work, let us first set out a framework and look at the AIDA data for the two limiting cases, namely $x = 0.5$, completely liquid AHS solution droplets, and $x = 1$, already well-studied pure AS crystals. The AIDA measurement data are contained in four different panels for each expansion cooling experiment (Figure 3). Panel (I) includes pressure and mean gas temperature, panel (II) the temporal evolution of S_{ice} and S_{liq}, panel (III) the OPC single particle measurements and the ice-active

Table 1
Summary of the Observed Crystallization Behavior and Ice Nucleation Mode for the Experiments With Fixed Particle Composition

Neutralization degree (x)	Particle phase/composition	Ice nucleation mode	S_{ice} threshold for $f_{ice} = 0.1\%$
0.5	Aqueous solution droplets	Homogeneous freezing	1.60
0.55	~35% aqueous solution droplets + ~65% AHS/LET crystals	Immersion freezing, followed by homogeneous freezing	1.52
0.6	AHS/LET crystals	Immersion freezing, followed by homogeneous freezing	1.45
0.675	AHS/LET crystals	Immersion freezing, followed by homogeneous freezing	1.52
0.75	≥95% LET crystals + ≤5% AHS/AS crystals	Deposition nucleation/PCF (possible small contribution of immersion freezing by the AHS/AS crystals)	1.35
0.8	LET/AS crystals	Deposition nucleation/PCF	1.37
0.9	LET/AS crystals	Deposition nucleation/PCF	1.39
1	AS crystals	Deposition nucleation/PCF	1.25

Note. The first column denotes the neutralization degree x of the bulk solution used for aerosol particle generation. The second column indicates the phase state and composition of the particles after the nebulized solution droplets were dried to RH typically ≤3% at 298 K and then injected into the AIDA chamber at 223 K and 31%–38% RH. The third column denotes the mode of ice nucleation that was observed in the AIDA expansion cooling runs. The fourth column indicates the threshold value for the ice saturation ratio at which the ice-active fraction exceeded a value of 0.1% during the AIDA experiments.

fractions derived from them, and panel (IV) the records from the SIMONE light scattering instrument. For the latter, we do not only show the depolarization ratio but also the total intensity of the laser light scattered at 2°, the second scattering angle detected by SIMONE (Schnaiter et al., 2012). The initial depolarization ratio of the

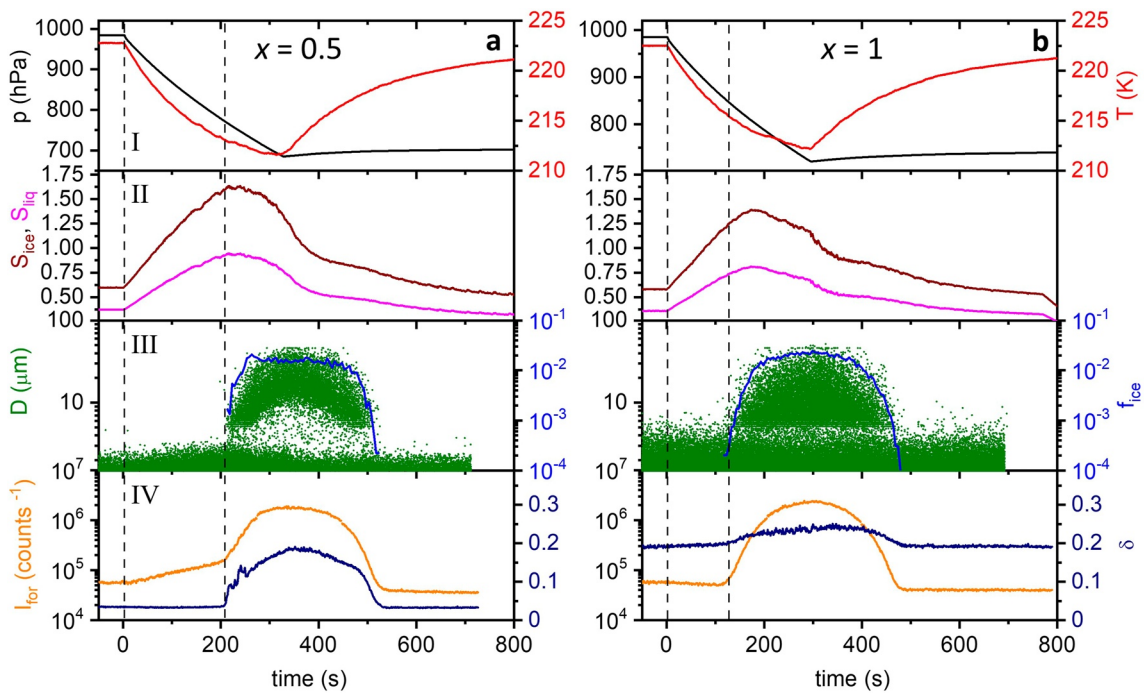

Figure 3. Aerosol Interaction and Dynamics in the Atmosphere (AIDA) expansion cooling experiments with aqueous ammonium bisulfate solution droplets ($x = 0.5$, part (a)) and ammonium sulfate crystals ($x = 1$, part (b)). The time series of the measurement data, where time zero indicates the start of pumping, are contained in panels (I–IV). I: AIDA pressure (black) and mean gas temperature (red). II: Saturation ratios with respect to ice (S_{ice}, brown) and supercooled liquid water (S_{liq}, magenta). III: Optical particle diameters inferred from the single-particle scattering signals of the optical particle counters (green dots) and ice-active fraction of the aerosol population (f_{ice}, blue line). IV: Light-scattering measurements with the Scattering intensity measurements for the optical detection of ice instrument. Forward scattering intensity at 2° scattering angle (I_{for}, orange) and depolarization ratio at 178° scattering angle (δ, dark-blue). Vertical dashed lines indicate prominent events during expansion cooling and are discussed in Section 3.1.2.

aqueous AHS particles is about 3%. Such a small non-zero residual, even for homogeneous spheres, is due to less than 100% linear polarization of the incident laser light and less than 100% efficient separation between the two polarization components of the backscattered light. A similar residual value of 3% for the depolarization ratio was also observed for the liquid sulfuric acid solution droplets injected at the beginning of the in situ neutralization experiment, and we take this value as baseline for completely liquid particles. After the start of expansion cooling at $t = 0$ (first vertical line), the AIDA data for $x = 0.5$ show the typical behavior for a homogeneous freezing experiment. The gradual increase in RH leads to water uptake by the aqueous particles, and the associated increase in particle size leads to a continuous increase in the total scattering signal at 2°, while the depolarization ratio remains constant at its background value. The increase in droplet size is also evident from the OPC records in panel (III). At a threshold of $S_{ice} = 1.6$ (second vertical line), we see the onset of the homogeneous freezing mode by the appearance of large ice crystals in the OPC records and a further strong increase in the scattering intensity at 2°. The ice crystals have a narrow distribution of particles sizes, since they nucleated at practically the same time at the same supersaturation threshold and therefore grew to a similar size and crystal shape. The ice cloud causes a temporary increase in the depolarization ratio until it falls back to the baseline of 3% when all aspherical ice crystals are sublimated after the stop of expansion cooling.

The initial depolarization ratio for crystalline AS particles ($x = 1$) was 19%. In contrast to the AHS solution droplets, there is no immediate water uptake by the AS crystals after the start of expansion cooling, which would cause an increase in the scattering signal at 2°; it even decreases slightly as the particle number concentration is reduced by the pumping. According to the OPCs, the size of the AS crystals is seemingly larger than that of the aqueous AHS solution droplets. However, this is not really the case and is due to the fact that the size of the aspherical AS crystals is overestimated in the OPC records, whose size classification is strictly valid only for spheres in the framework of Mie theory. At scattering angles between 78 and 102° covered by the OPCs, aspherical particles scatter more light than equivalent spheres, so they are assigned a larger optical diameter (Liu et al., 2006). Heterogeneous ice formation by crystalline AS in the deposition nucleation/PCF mode starts at a threshold value of about $S_{ice} = 1.25$ (f_{ice} threshold 0.1%, second vertical line), that is, far below the homogeneous freezing onset. S_{ice} rises to a maximum value of about 1.4, after which the supersaturation is slowly depleted by the high number of nucleated ice crystals, even with continued pumping. The ice-active fraction reaches a peak of 2%–3%. The distribution of ice crystal sizes for the heterogeneous freezing experiment with AS is much broader compared to the homogeneous freezing run with AHS because the ice crystals nucleated over a larger time range and thus in a larger range of ice supersaturations. As a high absolute number of ice crystals were formed in the expansion run with AS, all of which compete for the available water vapor and limit the maximum size to which each individual crystal can grow, the maximum diameters of the heterogeneously formed ice crystals (Figure 3b) do not differ significantly from those of the homogeneously nucleated ice crystals in the experiment with AHS (Figure 3a). Note that the inferred OPC diameters could also be biased by differences in the shape of the ice crystals. The depolarization ratio hardly reacts to the additional formation of larger, aspherical ice crystals and returns to the original value after the ice cloud has dissipated.

3.1.3. Ice Nucleation Behavior of AS–LET–AHS Particles With Intermediate Neutralization Degree

In Figure 4, we show the ice nucleation behavior for three selected intermediate compositions of $x = 0.6$, $x = 0.75$, and $x = 0.9$. Other particle compositions studied, which are not explicitly shown, are later identified with one of the nucleation behaviors shown in this figure. For $x = 0.6$, a crystalline mixture of AHS and LET, we start with a high depolarization ratio of >10% and initially see no water uptake until about $S_{ice} = 0.90$ (RH = 54%) (second vertical line). Then, before we reach the range of ice-supersaturated conditions, we first observe some fluctuations and then a steady decrease in the depolarization ratio to a value of about 4.5% at $t = 200$ s. At the same time, there is a small stepwise increase in the total scattering intensity and, as shown later, liquid water can be detected in the FTIR extinction spectra. The RH value of 54% therefore corresponds to the onset of the deliquescence of the AHS/LET particles at low temperature (219 K) and is the threshold where the AHS fraction of the particles goes into solution. The oscillations in the depolarization ratio point to a series of complex, intermediate particle morphologies in the initial part of the dissolution process. AHS could be distributed in the composite AHS/LET particle in different islands, and dissolution could start in different places and slowly form an aqueous particle with the still undissolved LET fraction in its core. Such a final particle morphology would be consistent with the small, above-baseline value for the depolarization ratio obtained at $t = 200$ s during expansion cooling. However, we cannot say for sure whether the LET portion is present as a single, compact crystalline core or as smaller fragments. Before the immersed LET crystals could completely dissolve, some of the internally mixed solid-liquid

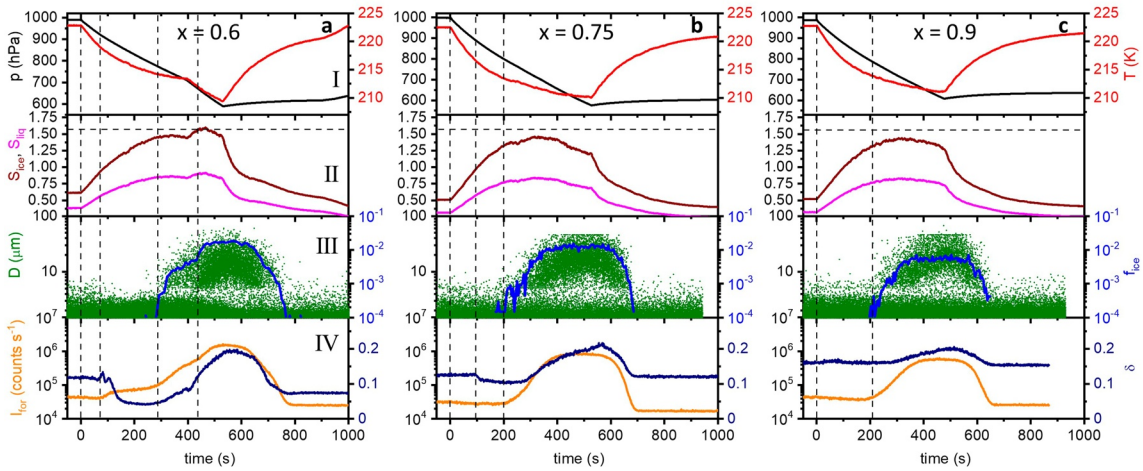

Figure 4. Aerosol Interaction and Dynamics in the Atmosphere expansion cooling experiments with ammoniated sulfate particles of intermediate neutralization degree (part a: $x = 0.6$, part b: $x = 0.75$, and part c: $x = 0.9$). The individual panels (I–IV) show the same data types as in Figure 3. The horizontal dashed line in panels II indicates the homogeneous freezing threshold observed in the experiment with aqueous ammonium bisulfate solution droplets (Figure 3a). The events associated with the vertical dashed lines are discussed in Section 3.1.3.

particles induced ice formation in the immersion freezing mode, starting at about $S_{ice} = 1.45$ (third vertical line). As the heterogeneously formed ice crystals began to deplete the supersaturation, we increased the pumping speed at $t = 400$ s and were also able to exceed the homogeneous freezing threshold where a second ice nucleation mode occurred (fourth vertical line). To guide the eye, the homogeneous freezing threshold observed for aqueous AHS solution droplets (Figure 3a) is shown as a dashed horizontal line in panels II of Figure 4. After sublimation of the ice crystals, the depolarization ratio relaxed to a value of only 7%, indicating that part of the AHS/LET particles had completely deliquesced during the expansion run. Otherwise, if a small solid LET core had remained in each particle at the end of expansion cooling, it would likely have triggered complete recrystallization as soon as the relative humidity dropped below the threshold value for the partial deliquescence of the AHS fraction at 54%. In this case, depolarization would have returned to its original value.

The FTIR measurements can be used to support the interpretation of the initial deliquescence behavior of the AHS/LET particles. Panel (a) in Figure 5 shows the FTIR spectra recorded in the initial period of the expansion run for mixed AHS/LET particles with $x = 0.6$. The black colored spectra were recorded during the phase when the RH increased from 38% to 52%. They remain unchanged, indicating that the crystalline particles here do not absorb water. The liquid water signature starts to appear in the red colored spectrum recorded at 54% RH, indicating the onset of deliquescence. Complete dissolution of the AHS portion in the mixed AHS/LET crystals and growth of the aqueous layer around the not yet fully dissolved LET portion leads to a further increase of the liquid water extinction signal at higher RH (blue spectra). For aqueous AHS particles ($x = 0.5$, panel b), significant water uptake occurs when the humidity is increased from 37% to 54%. The absence of any heterogeneous ice formation and low initial depolarization ratio indicate that the particles were indeed completely liquid (see Figure 3a). We can therefore use these spectra to scale the corresponding infrared measurements from the experiment for $x = 0.55$ (panel c), where we had already mentioned that the particles were not completely aqueous. For $x = 0.55$, the liquid water signature at RH = 37% and the amount of water absorbed up to 54% RH is only about 35% of the values observed for $x = 0.5$, leading to our conclusion above that about 35% of the particles were liquid and 65% were a crystalline mixture of AHS and LET. In agreement with the presence of a considerable fraction of solid particles, we also observed an immersion freezing mode for $x = 0.55$, as shown in Figure 4a for $x = 0.6$. The same applies to the crystalline mixture of AHS and LET with $x = 0.675$ (Table 1). The AIDA data for these two experiments are shown in Figure S1.

Pure LET particles ($x = 0.75$) should deliquesce at a relative humidity of not less than 73% RH (Colberg et al., 2003). However, in the AIDA data of the expansion cooling experiment with $x = 0.75$ (Figure 4b), we see a small stepwise decrease in the depolarization ratio already at 56% RH (second vertical line), coinciding with the relative humidity threshold where the AHS fraction in the experiment with $x = 0.6$ began to dissolve. This is consistent with the finding of Rosenoern et al. (2008) that for $x = 0.75$, a small fraction of mixed AS/AHS

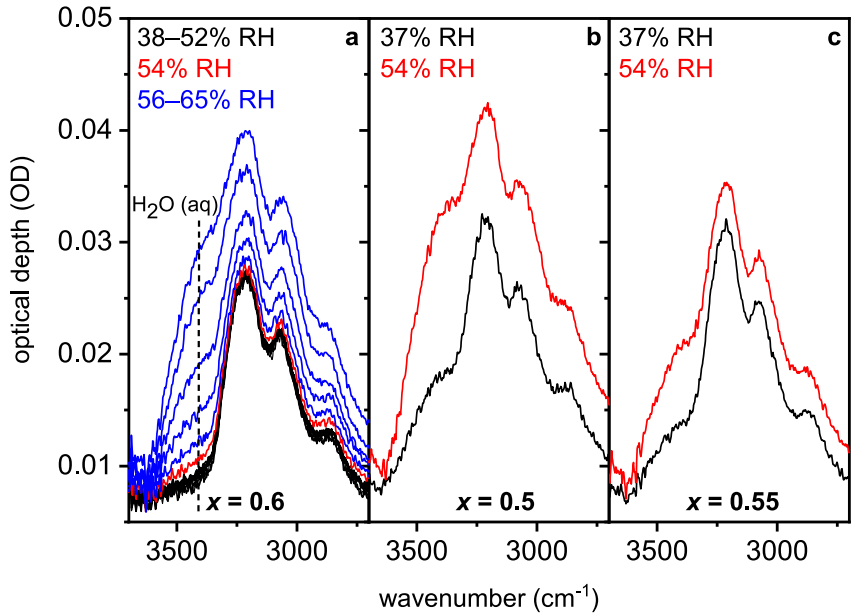

Figure 5. Detailed view of the infrared extinction signature due to liquid water in the initial phase of the expansion cooling experiments with ammoniated sulfate particles of the compositions $x = 0.6$ (part a), $x = 0.5$ (part b) and $x = 0.55$ (part c). The color coding of the spectra indicates the RH conditions in the Aerosol Interaction and Dynamics in the Atmosphere chamber under which the spectra were recorded. Further details are given in Section 3.1.3.

particles forms in addition to pure LET. Based on the amount of liquid water that appeared in the FTIR data at RH > 56% in comparison with the spectra shown in Figure 5a for $x = 0.6$, we estimate the AS/AHS fraction to be ≤5%. The heterogeneous freezing mode with a maximum ice-active fraction of 2% starting at about $S_{ice} = 1.35$ ($f_{ice} = 0.1\%$, third vertical line) is therefore mainly due to deposition nucleation/PCF on LET, but could also be, to a minor extent, immersion freezing by AS. During the entire course of expansion cooling, S_{ice} never exceeded the homogeneous freezing threshold. The general behavior of the AIDA data in the expansion cooling run with $x = 0.9$ (Figure 4c), representing a crystalline mixture of LET and AS, is identical to the AS-only experiment and reveals a deposition nucleation/PCF ice mode without prior notice of partial deliquescence. The same applies to the experiment with $x = 0.8$ (Table 1, Figure S1).

3.1.4. Summary of the Composition-Dependent Ice Nucleation Behavior in the AS–LET–AHS System

After the detailed phenomenological discussion of the individual AIDA experiments, we conclude this section with two overview graphs quantifying the continuous change of the ice nucleation behavior in the AS–LET–AHS system when the particle composition is changed from $x = 0.5$ to $x = 1$ (Figures 6a and 6b). In panel (a), we show the S_{ice}—T trajectories for the five experiments explicitly discussed above with superimposed dots whose sizes indicate the ice-active fractions at different stages of expansion cooling. A representation of the ice-active fractions as a function of S_{ice} for all AIDA experiments performed is shown in panel (b). As illustrated by the color coding, the results suggest that four different categories of particles should be considered with respect to the ice nucleation behavior. Category 1 are pure AS particles ($x = 1$, red), characterized by the clearly lowest onset S_{ice} value for deposition nucleation/PCF. Category 2 are mixed LET/AS and pure LET particles in the range from $x = 0.9$ to $x = 0.75$ (yellow-orange colors). Here, the AIDA data suggest that the particle surfaces are somewhat less susceptible to ice formation in the deposition nucleation/PCF mode compared to AS, resulting in a horizontal shift of the f_{ice} versus S_{ice} curves by an absolute amount of about 0.1 to higher S_{ice} values. Category 3 are mixed AHS/LET particles in the range from $x = 0.675$ to $x = 0.55$ (greenish colors). Such particles can still initiate heterogeneous ice formation due to the immersed LET crystals that do not completely dissolve during expansion cooling. However, the onset of ice nucleation shifts further to higher S_{ice} values and the maximum ice-active fractions before reaching homogeneous freezing conditions are below 1%, that is, lower than for particle compositions where the deposition nucleation/PCF mode is active. This is consistent with previous studies where poor heterogeneous ice nucleation ability was observed for immersed LET crystals (Chen et al., 2000; Zuberi et al., 2001). Category 4 are aqueous AHS particles ($x = 0.5$, blue), which we found do not crystallize and therefore form ice only by homogeneous freezing.

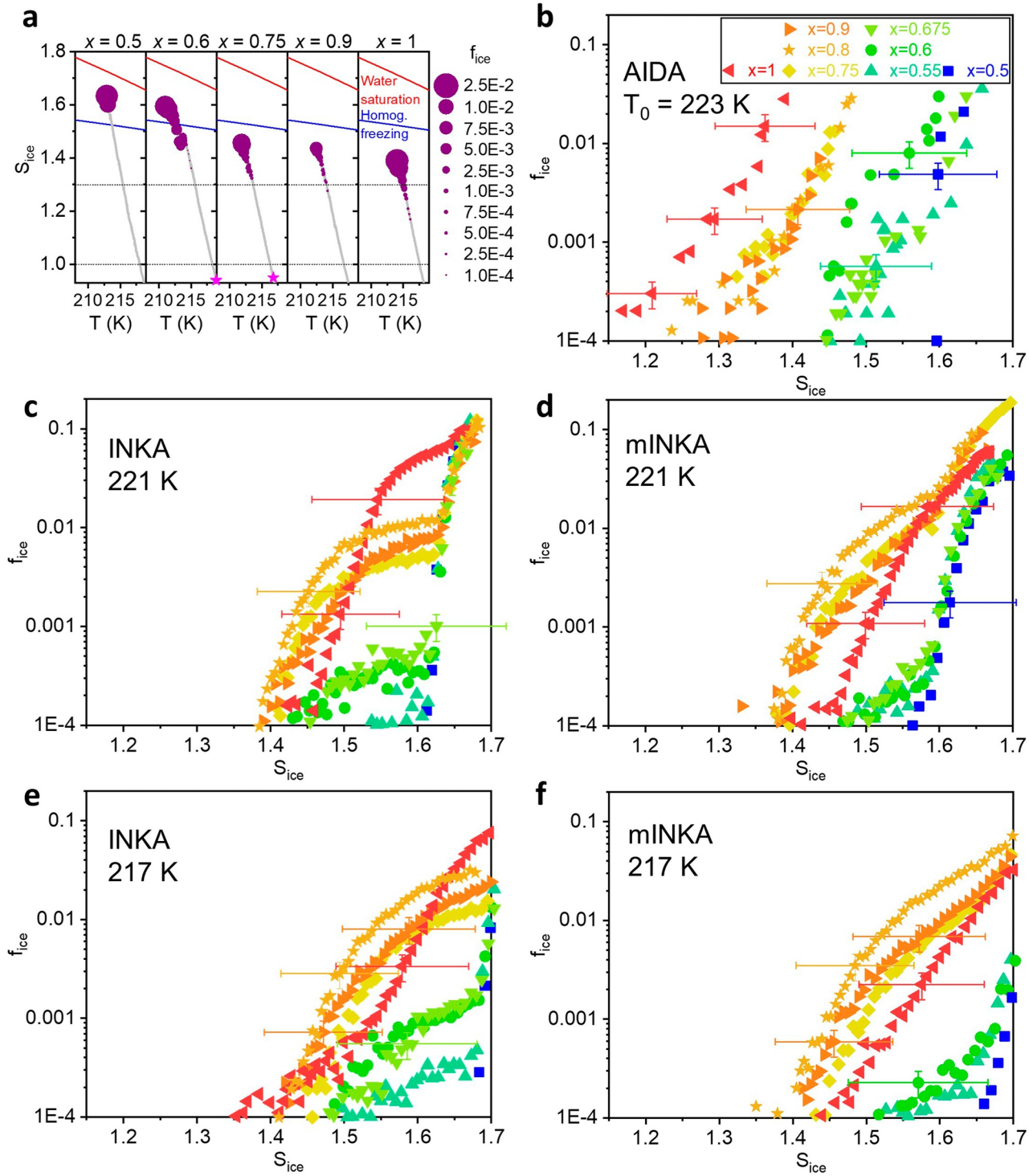

Figure 6. Ice nucleation behavior of ammoniated sulfate particles as a function of the degree of neutralization x. (a) S_{ice} versus T trajectories of the Aerosol Interaction and Dynamics in the Atmosphere (AIDA) expansion cooling experiments discussed in Section 3.1, where the size of the superimposed points indicates the ice-active fraction, f_{ice}. The pink stars in the experiments for $x = 0.6$ and 0.75 denote the observed deliquescence onset of the ammonium bisulfate particle fraction. Homogeneous freezing conditions (Koop et al. (2000), blue) and water saturation (red) are also shown. (b)–(f) Ice-active fractions as a function of S_{ice} for the AIDA expansion experiments, which started at 223 K, and the Ice Nucleation Chamber of the Karlsruhe Institute of Technology and mINKA humidity scans, which were performed at 221 and 217 K. The legend of panel b refers to all sub-panels thereafter. Due to technical problems with mINKA, no data is available for $x = 0.675$ at 217 K.

3.2. Comparison Between the AIDA and the CFDC (INKA and mINKA) Ice Nucleation Measurements

The general ice nucleation behavior observed in the AIDA measurements is largely confirmed by the INKA and mINKA f_{ice} data shown in Figures 6c–6f for two different temperatures (221 and 217 K). Category 4 particles ($x = 0.5$) exclusively show the homogeneous freezing mode, while category 3 particles ($x = 0.675$ to $x = 0.55$) reveal a small immersion freezing mode prior to the homogeneous freezing onset. Ice formation in the deposition nucleation/PCF mode by category 1 ($x = 1$) and category 2 ($x = 0.9$ to $x = 0.75$) particles initiates at the lowest S_{ice} thresholds. However, the CFDC data do not point towards a superior heterogeneous ice nucleation ability of pure AS compared to less neutralized particles, that is, they do not support the division into category 1 and category 2 particles as indicated by the AIDA measurements. The error bars with respect to S_{ice} in the AIDA data (Figure 6b) reflect the uncertainty in the TDL measurements, which is dominated by the uncertainty in the line strength of the scanned water vapor absorption line (Fahey et al., 2014). Since the same absorption line is always used, we assume that the relative difference in the f_{ice} versus S_{ice} curves between individual AIDA measurements is significant, that is, that the distinction by category 1 and category 2 particles is sound. The error bars with respect to S_{ice} in the INKA and mINKA data (Figure 6c–6f) reflect the uncertainty in temperature and in the gap width between the two cylindrical walls of the diffusion chambers, which is governed by the estimated thickness of the deposited ice layers (Rogers, 1988; Schiebel, 2017). Each INKA and mINKA measurement for a specific particle composition x in the AS–LET–AHS system required a new conditioning (cooling and icing of the cylindric walls) of the respective CFDC chamber. Small relative differences in the ice nucleation ability between different particle compositions, for example, the distinction between category 1 and category 2 particles, are therefore difficult to detect, as we always have to take into account the full absolute uncertainty in S_{ice} for the individual measurements. The situation would be different if the CFDC chambers did not have to be reconditioned between experiments, that is, if repeated humidity scans were performed with well-conditioned INKA and mINKA instruments while only the particle composition x changed. This is exactly the procedure of the additionally performed in situ neutralization experiment, which is described in the next section.

Apart from the question of distinguishing between category 1 and category 2 particles, the data from Figures 6b–6f show that the nucleation onsets are typically lower in the AIDA expansion cooling experiments than in the measurements with the two CFDC chambers. This is similar to our earlier comparative study of AIDA and INKA ice nucleation measurements with ammonium nitrate particles under cirrus conditions (Wagner et al., 2020). We have identified a number of possible explanations for this, which we will only briefly summarize here, and refer to our recent publication for a more in-depth discussion (Wagner et al., 2020). On the one hand, the AIDA nucleation onsets could be susceptible to a negative bias in terms of S_{ice} because small, turbulent air parcels (eddies) could be formed during expansion cooling. Such eddies, where the temperature could be lower than the recorded mean AIDA gas temperature, resulting in a locally higher S_{ice} value, might be the starting point of the nucleation process, so that the S_{ice} onset calculated from the mean gas temperature has a negative bias. For the CFDC measurements, it is important to know that an RH ramp does not mean continuous RH processing of the same INPs as it takes place during the AIDA expansion experiments. While the CFDC instruments are adjusted to a new ice supersaturation value by slowly changing the wall temperatures during the RH ramps, they are continuously flushed with fresh INPs from the AIDA chamber. Therefore, the entire process of nucleation and ice crystal growth to sizes detectable by the OPCs must be completed within the short particle residence time of $\leq$10 s. This could induce a positive bias of the CFDC data in terms of S_{ice} in comparison with the AIDA results for which longer observation times apply, that is, a higher ice supersaturation than prevalent in the AIDA chamber might be required to accelerate the nucleation and growth process in the CFDCs and to observe the same number concentration of ice crystals as in the cloud chamber.

3.3. CFDC Ice Nucleation Measurements From the In Situ Neutralization Experiment

The in situ neutralization experiment began with the injection of sulfuric acid solution droplets ($x = 0$) into the AIDA chamber, which was maintained at 223 K and 25% RH. With the start of NH_3 addition, the aerosol particles first remained in the liquid phase until the ammonium content exceeded the stoichiometry of AHS ($x = 0.5$). Excess ammonium could then lead to precipitation of LET, which in turn served as a nucleus for crystallization of the residual liquid, forming mixed AHS/LET crystals. Further neutralization due to continued NH_3 addition then proceeded in the solid phase. The particle composition was deduced from the simultaneous FTIR measurements. The infrared spectra recorded during the in situ neutralization experiment were thereby

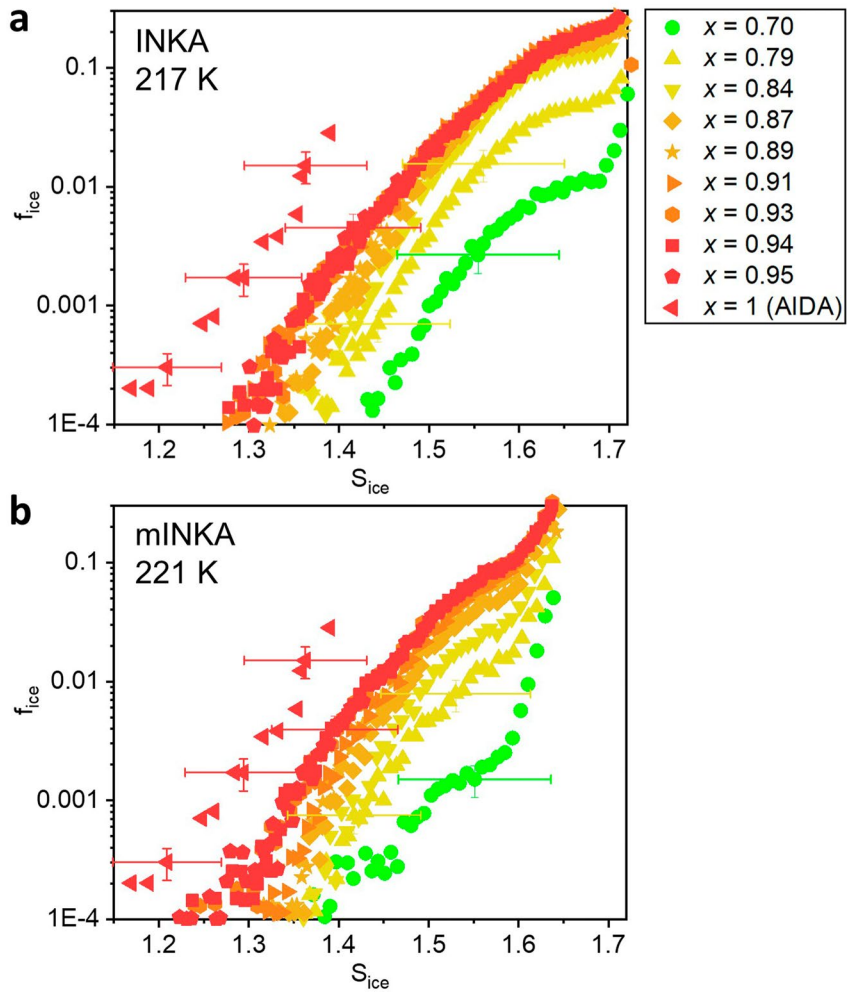

Figure 7. Composition-dependent ice nucleation behavior of the ammoniated sulfate particles during the in situ neutralization experiment, measured with Ice Nucleation Chamber of the Karlsruhe Institute of Technology at 217 K and mINKA at 221 K. The degree of neutralization x was derived from the infrared extinction spectra recorded simultaneously. The ice-active fractions measured during the expansion cooling experiment with pure ammonium sulfate particles ($x = 1$) are shown for comparison.

best fitted in the wavenumber range from 1,600 to 1,000 cm^{-1} by a linear combination of the basis spectra measured during the experiments with fixed particle composition (Figure 2). Panels (a) and (b) of Figure 7 show the evolution of the ice nucleation ability of the particles during neutralization, recorded with INKA at 217 K and with mINKA at 221 K, respectively. The green dots show the CFDC measurements for a particle composition of $x = 0.7$. In agreement with the discussion from Sections 3.1 and 3.2, the humidity scans for these mixed AHS/LET crystals show an immersion freezing mode followed by homogeneous freezing. More frequent CFDC scans were then performed for $x \geq 0.75$, because, as emphasized in Section 3.2, the focus of this experiment was to study more accurately the relative change in the efficiency of ice nucleation in the deposition nucleation/PCF mode for particles with compositions between $x = 0.75$ and $x = 1$. The CFDC humidity scans show that there is a continuous horizontal shift of the f_{ice} versus S_{ice} traces towards lower nucleation onsets as the particle composition changes from LET to AS stoichiometry. Although the absolute error of S_{ice} in the individual measurements is comparable to the observed shift in the nucleation onsets, we strongly believe that the relative trend detected by the CFDCs is well-founded, as the repeated measurements did not require reconditioning of the instruments, but were performed with identical settings. Furthermore, the same relative trend was observed with both CFDC instruments and the result is consistent with the observations from the AIDA expansion cooling experiments (Figure 6b). The final INKA and mINKA humidity scans for $x = 0.95$ show good agreement with the activated fraction curve from the AIDA experiment with pure AS ($x = 1$), whose data are included in Figure 7 for

comparison. Note that the AIDA data have a lower maximum value for S_{ice}, which is due to the depletion of the supersaturation later in the expansion cooling process.

Both the AIDA expansion runs and the in situ crystallization experiment prove that the fully neutralized AS crystals are the most efficient INPs. How this can be explained on a microscopic level remains a matter of speculation. An interesting observation from the in situ crystallization experiment is the gradual shift of the f_{ice} versus S_{ice} curves in their entirety towards lower saturation ratios. For example, if we consider a particle with $x = 0.84$, the given value corresponds to the average particle composition. As far as the juxtaposition of the two solid phases LET and AS is concerned, it is plausible to think of a morphology in which the outer particle layers are, at least in parts, already completely neutralized to AS, because they are directly exposed to the NH_3 vapor, while the LET fractions tend to predominate in the center of the particles. However, these $x = 0.84$ particles do not show, even for a subset, the same onset of ice nucleation as the completely neutralized AS particles. From this, one could conclude that there are some relevant surface properties that still change with continued neutralization, and the further the particles are neutralized, the more they favor early heterogeneous ice formation. These particular surface properties could lie in the nature of chemical bonding, reducing the nucleation free energy barrier for deposition nucleation, or they could be suited pores and cracks that facilitate ice nucleation via the PCF mechanism.

3.4. Parameterization of the Ice Nucleation Behavior in the AS–LET–AHS System in Terms of n_s

The ice nucleation active surface site density (n_s) approach represents a simple empirical concept for quantifying the heterogeneous ice nucleation ability of aerosol particles. It involves normalization to the surface area of the particles and thus assumes that the particle composition or surface properties are uniform and size-independent (when applied to a polydisperse particle population), and it ignores time dependence (Connolly et al., 2009; Hoose & Möhler, 2012). We want to provide here an estimate for composition-dependent n_s densities in the AS–LET–AHS system. It should be noted that we do not have enough data to investigate in detail the temperature dependence of the n_s values over the entire range of cirrus temperatures. The dynamic temperature range covered by the AIDA expansion cooling runs started at 223 K overlaps with the two temperatures of 217 and 221 K at which the CFDC measurements were performed, and our derived n_s parameterizations are strictly valid only for this temperature range. However, in our previous work dealing with ice nucleation experiments with mixed ammonium nitrate/ammonium sulfate (AN/AS) crystals (Wagner et al., 2020), we found only a small temperature dependence of the ice nucleation onsets between 230 and 205 K, which could possibly also apply to the AS–LET–AHS system.

We now describe the procedure for deriving the n_s values and start our discussion with pure AS. Similar to our ice nucleation experiments in the AN–AS system just mentioned (Wagner et al., 2020), we created a combined f_{ice} versus S_{ice} curve from the AIDA and CFDC measurements. As shown in Figures 6b and 7, the AIDA data are only available up to a peak S_{ice} value of about 1.4. After that, the supersaturation in the gas phase was depleted by the large number of nucleated ice crystals, while the CFDC humidity scans reached saturated conditions with respect to water ($S_{ice} \approx 1.7$). So we took the AIDA f_{ice} data for $x = 1$ and extended them beyond $S_{ice} = 1.4$ with the data points from the last INKA scan of the in situ crystallization experiment (Figure 7a). The INKA f_{ice} curve was horizontally shifted by −0.1 on the S_{ice} scale to overlap with the AIDA data set. By dividing the combined AIDA and S_{ice}-shifted INKA f_{ice} data by the average surface area of the AS particles, we obtained the corresponding n_s data, which we then fitted by a polynomial function, as shown in Figure 8.

For mixed LET/AS ($1 < x < 0.75$) and pure LET ($x = 0.75$) particles, our ice nucleation data suggest that the general shape of the f_{ice} versus S_{ice} curves is similar to that for AS particles, but shifted horizontally towards higher S_{ice} values, with an absolute offset of about 0.1 between $x = 1$ and $x = 0.75$ (Figures 6b and 7). Assuming that this offset changes linearly between the AS and LET stoichiometry, as indeed indicated by the CFDC data in Figure 7, we can provide a general fitting function for the n_s density in the AS–LET system (category 1 and 2 particles defined in Section 3.1.4) that includes the degree of neutralization x as a parameter:

$$\log_{10} n_s = \left\{ a + b \cdot \left(S_{ice} - \frac{1-x}{2.5} \right) + c \cdot \left(S_{ice} - \frac{1-x}{2.5} \right)^2 + d \cdot \left(S_{ice} - \frac{1-x}{2.5} \right)^3 + e \cdot \left(S_{ice} - \frac{1-x}{2.5} \right)^4 \right\} \text{m}^{-2} \quad (1)$$

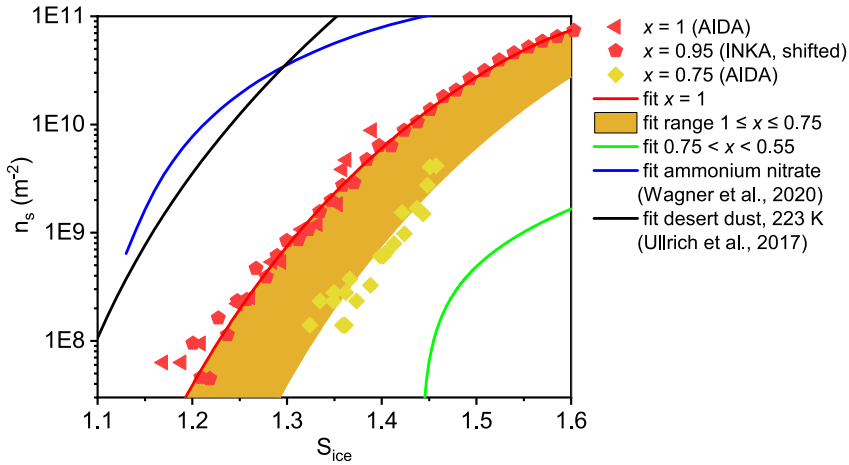

Figure 8. Parameterizations of the composition-dependent ice nucleation active surface site densities, n_s, for the AS–LET–AHS system derived in this work in comparison with n_s values for other aerosol particle types (ammonium nitrate, blue line; desert dust, black line). The orange area denotes the range of n_s values calculated with Equation 1 for $1 \leq x \leq 0.75$, where the red line represents an explicit computation for $x = 1$. The green line is the parametrization for neutralization degrees in the range $0.75 < x < 0.55$ (Equation 2). Underlying Aerosol Interaction and Dynamics in the Atmosphere and Ice Nucleation Chamber of the Karlsruhe Institute of Technology measurement data are marked by the symbols.

The term $\left(\frac{1-x}{2.5}\right)$ accounts for the horizontal shift of the S_{ice} curve for $x < 1$, with a maximum amount of 0.1 for LET ($x = 0.75$). Equation 1 is valid for S_{ice} between $\left(1.19 + \frac{1-x}{2.5}\right)$ and 1.6 (the homogeneous nucleation onset) and x between 0.75 and 1 with parameters given by: $a = -230.59333$, $b = 605.28421$, $c = -589.64156$, $d = 262.36387$, and $e = -44.57865$. The lower threshold value of $S_{ice} = 1.19$ corresponds to the detection limit with respect to n_s of about $3{\cdot}10^7$ m^{-2} in the measurement for $x = 1$. With a horizontal shift of the S_{ice} curve for $x < 1$, the lower S_{ice} threshold must therefore be increased accordingly. If we set $x = 1$, we obtain the red line in Figure 8, that is, the fitting curve for pure AS particles. The orange shaded area shows the range of n_s data when x is varied between 0.75 and 1. For comparison, we also included the n_s values derived from the AIDA expansion run for $x = 0.75$. We emphasize again that the orange shaded area was constructed by using the AIDA f_{ice} data as anchor points to which the CFDC data sets were fitted. This procedure remains a matter of debate and further work is needed to assess the differences between AIDA and CFDC results for ice nucleation measurements under cirrus conditions (Wagner et al., 2020). As noted above, a horizontal shift of +0.1 on the S_{ice} scale would bring the orange shaded area into the data range of the uncorrected CFDC measurements (Figure 7). This allows modelers to perform a sensitivity analysis to determine how the discrepancies between the AIDA and CFDC data affect the model results.

For mixed AHS/LET particles (category 3 particles, $0.75 < x < 0.55$), the heterogeneous ice nucleation ability is much smaller and proceeds via the immersion freezing mode. Theoretically, one would expect the ice-active fraction to increase with x, that is, with the size of the LET core, which initially remains undissolved after the dissolution of the AHS fraction. However, the AIDA and CFDC data do not reveal such a systematic trend, and we therefore provide a fitting function to the average n_s values from the three individual AIDA expansions experiments conducted for $x = 0.55$, $x = 0.6$, and $x = 0.675$:

$$n_s = a + b \cdot \exp\left\{\frac{(S_{ice} - c)}{d}\right\} \text{ m}^{-2} \quad (2)$$

Equation 2 applies to S_{ice} between 1.445 and 1.6 and should be considered representative of the n_s values in the AHS–LET system for $0.75 < x < 0.55$, where the parameters are as follows: $a = -1.70889{\cdot}10^9$, $b = 1.12514{\cdot}10^9$, $c = 1.34383$, and $d = 0.23361$. The fitting function can be seen as the green curve in Figure 8. We emphasize that the n_s values for the mixed AHS/LET particles are obtained by normalization with respect to the dry particle surface area. The train of thought behind this approach is that the entire dry particle surface is in principle available as an ice nucleation surface, similar as for crystals in the LET–AS system. The special hygroscopic behavior of the AHS/LET particles, however, prevents this available surface area from triggering ice formation in the

deposition nucleation/PCF mode. Instead, partial deliquescence takes place and only enables ice nucleation in the immersion freezing mode. A different approach to obtaining n_s would be the normalization to the residual size of the solid LET core that actually initiates the immersion freezing mode. However, we have no means to accurately determine its size, as we cannot rely on the Extended Aerosol Inorganic Model (E-AIM) because it does not seem to correctly reproduce the hygroscopic behavior of the AHS/LET particles at low temperatures (see Section 3.5).

We also included in Figure 8 our recent n_s parameterization for almost pure AN particles crystallized from 99.4 mol% AN + 0.6 mol% AS solution droplets (blue line; Wagner et al., 2020). These almost pure AN particles, which could only be crystallized by adding the small amount of AS, revealed the lowest ice nucleation onsets in the AN–AS system, while increasing the AS content led to similar nucleation onsets as for pure AS particles (Wagner et al., 2020). The range between the blue and the red line in Figure 8 can thus be regarded as representative of crystalline, mixed particles in the AN–AS system. Lower ice nucleation onsets compared to pure AS, similar to those of almost pure AN particles, are also predicted by a n_s parameterization for desert dust aerosol particles (Figure 8, black line) (Ullrich et al., 2017).

A general word of caution should be said about the validity of the n_s concept. Our experiments focused on the composition-dependent ice nucleation behavior for a fixed particle size (achieved by always using the same mass of solutes to prepare the bulk solutions), and we did not look further into size-dependent measurements to confirm whether the same n_s values are obtained for different particle sizes or surface areas. For crystalline ammonium nitrate, it was found that the n_s parameterization derived from AIDA expansion experiments with 810–960 nm sized particles (Wagner et al., 2020) is also applicable to mINKA ice nucleation measurements from CERN CLOUD nucleation studies with particles of <100 nm (M. Wang et al., 2022). However, for other crystalline inorganic compounds, namely SSA particles and sodium chloride (NaCl) crystals, it has recently been observed that ice formation at cirrus temperatures occurs with the same efficiency regardless of aerosol size or apparent geometric surface area (Patnaude et al., 2021). In Patnaude et al. (2021), 150 and 600 nm particles were investigated. The comparatively large particle size of 900 nm in our study was chosen to achieve good mass loading for infrared measurements and a detectable depolarization ratio so that phase changes of the particles during expansion cooling could be clearly followed. If what Patnaude et al. (2021) observed also holds for the AS–LET–AHS system, and smaller particles have the same IN efficiency, that is, ice-active fraction, as the 900 nm particles studied, our derived n_s data would have to be considered lower estimates, as dividing by a smaller particle surface area would yield higher n_s values. This undoubtedly important question must be clarified in future experiments.

3.5. Deliquescence Behavior of AS–LET–AHS Particles at Low Temperatures

In addition to the ice nucleation results, our experiments provide new insights into the deliquescence behavior of particles in the AS–LET–AHS system at low temperatures, which we briefly summarize here. From the AIDA expansion cooling experiments, the following values were obtained for the onset of deliquescence of the AHS fraction in mixed crystalline AHS/LET particles at low temperature (≈220 K): 55% RH for $x = 0.55$ (applies to the crystalline particle fraction), 54% RH for $x = 0.6$, and 64% for $x = 0.675$. The larger LET fraction for $x = 0.675$ could shield the AHS islands in the composite particles and delay water uptake, explaining the higher deliquescence onset (Mifflin et al., 2009). For the small fraction of mixed AHS/AS crystals in the experiment for $x = 0.75$, we observed the deliquescence onset for the AHS fraction at 56% RH. The increase in the deliquescence onset at lower temperatures compared to the room-temperature measurement of 39% RH (Spann & Richardson, 1985) is not accurately captured by the Extended AIM Aerosol Thermodynamics Model (Clegg et al., 1998), where the onset of deliquescence of the AHS fraction in mixed crystalline AHS/LET particles is predicted to occur at 37% RH down to a temperature of 230 K. As the phase state of the aerosol particles (i.e., aqueous or solid) affects light scattering properties and chemical reaction rates (Martin et al., 2004), this modified low-temperature deliquescence behavior should be considered in future model simulations. The relative humidity for complete dissolution of the mixed AHS/LET particles at low temperatures is difficult to determine. We have addressed above the SIMONE depolarization observations that during the AIDA expansion run for $x = 0.6$ a subset of the particles completely deliquesced (Section 3.1.3). RH reached a maximum value of 89% in that run, which could thus indicate the approximate threshold for the full DRH.

Regarding the deliquescence onsets for LET/AS particles with $x > 0.75$, we can refer to the CFDC measurements where the humidity scans were forced to reach 100% RH, so that particles not acting as INPs will eventually

deliquesce. The uptake of water when the onset of deliquescence is exceeded results in particle growth and can be detected by analyzing the count rates in individual size channels of the OPC connected to the outlet of the CFDCs (Kong et al., 2018; Wagner et al., 2020). From the INKA and mINKA measurements at 221 K, we inferred deliquescence onsets in the range of 92%–94% RH for particles with $0.75 < x \leq 1$. At this temperature, the predictions of the Extended AIM Aerosol Thermodynamics Model are in the range of 85%–86% RH, that is, still within the uncertainty limit of the RH values derived from the CFDC measurements.

4. Conclusions

The efficiency of heterogeneous ice nucleation in the AS–LET–AHS system reveals a strong dependence on the particle composition. Pure AS crystals show the lowest ice nucleation onset ($S_{ice} = 1.20$–1.25 for $f_{ice} = 0.01$–0.1%) when probed in expansion cooling runs in the AIDA cloud chamber, which is consistent with the chosen threshold for heterogeneous ice nucleation by AS in recent model simulations (Beer et al., 2022; Penner et al., 2018). Crystalline, ammoniated sulfate particles remain efficient INPs in the deposition nucleation or PCF mode for a neutralization degree down to 0.75, but the nucleation onsets gradually shift to $S_{ice} = 1.30$–1.35. A more pronounced change occurs at a neutralization degree $x < 0.75$ where the particles are mixed crystals composed of LET and AHS. The AHS fraction dissolves prior to reaching ice supersaturated conditions, changing the mode of ice nucleation from deposition nucleation/PCF to immersion freezing by the not yet fully dissolved LET portion. The efficiency of ice formation in terms of nucleation onset, ice-active fraction and ice nucleation active surface site density is then much lower than for particle compositions where the deposition nucleation/PCF mode is active.

That aqueous particles with an immersed LET core are more likely to be ice inactive is consistent with previous studies (Chen et al., 2000; Zuberi et al., 2001), but differs from the behavior of another type of inorganic INP, namely SSA particles. SSA particles show a gradual deliquescence behavior, and, when reaching ice supersaturated conditions, they are expected to be mixed-phase solid-liquid particles with an aqueous layer of dissolved salts around a solid core of not yet fully dissolved NaCl (Schill & Tolbert, 2014). In this system, heterogeneous ice formation in the immersion freezing mode by the SSA particles at temperatures below about 220 K proved to be as efficient as deposition nucleation/PCF ice formation on crystalline NaCl particles (Patnaude et al., 2021; Wagner et al., 2018).

At a neutralization degree of 0.55, aqueous AHS/LET particles no longer crystallize with 100% efficiency when exposed to a relative humidity of ≤3% at 298 K. With pure AHS solution droplets ($x = 0.5$), no crystallization occurs at all. Ice formation can then only take place through homogeneous freezing. Our data allow for the first time a more differentiated treatment of ice formation by ammoniated sulfate particles depending on their degree of neutralization in future model runs. It is useful to remind here the study of Nault et al. (2021), which provides a comprehensive overview of the ammonium balance around the globe from atmospheric observations (data from 11 aircraft campaigns using the Aerodyne Aerosol Mass Spectrometer) and includes a comparison of the observation data with nine different CTMs. Note that the ammonium balance defined in Nault et al. (2021) not only includes the fractional charge neutralization of sulfate, but also of nitrate and chloride. The authors found that the CTMs predicted complete neutralization at all locations and altitudes over continental regions, while the observations indicated systematically lower neutralization levels at <400 hPa in the upper troposphere and >50–60°N, the latter indicating a lower ammonia source in boreal forests compared to air masses over more polluted continental regions. In addition, the regions with a high ammonium balance over the Pacific and the Atlantic are spatially less extensive in the observations compared to the models. Further observational data are required to substantiate these results, which will then indicate how often ice nucleation parameterizations for sulfate particles that are not completely neutralized by ammonium need to be used.

In addition to incomplete neutralization, mixing with organic matter can also lead to a change in the heterogeneous ice nucleation ability of AS, due to a number of factors that were already briefly addressed in the introduction. First of all, a high organic mass fraction could possibly inhibit the crystallization of aqueous AS solution droplets and prevent them from becoming INPs. When highly viscous organic components condense on an already crystallized AS particle, the ice-active inorganic solid is shielded and loses its ice activity. Immersion freezing by crystalline AS particles embedded in less viscous organic solutions proved to be less efficient than deposition nucleation/PCF ice formation on the bare crystals. We thus see that all compositional changes with respect to pure AS, that is, a reduction in the degree of neutralization and mixing with organic matter, have a

common direction in which the heterogeneous ice nucleation behavior develops, namely a deterioration of that of the bare, completely neutralized crystals. Parameterizations of ice nucleation for AS alone are therefore insufficient to capture the entire family of pure or internally mixed ammoniated sulfate particles and could potentially lead to overprediction of ice formation.

Data Availability Statement

The processed data used to derive the parametrizations for the ice nucleation active surface site densities in this work are the composition-dependent ice-active fractions in the AS-LET-AHS system measured with AIDA and the two CDFCs. These data are available in KITopen (RADAR4KIT repository) at https://doi.org/10.35097/1847 (Bertozzi et al., 2023).

Acknowledgments
We gratefully acknowledge the continuous support by all members of the Engineering and Infrastructure group of IMK-AAF, in particular by Olga Dombrowski, Rainer Buschbacher, Tomasz Chudy, Jens Nadolny, Steffen Vogt, and Georg Scheurig. This work has been funded by the Helmholtz-Gemeinschaft Deutscher Forschungszentren as part of the program "Atmosphere and Climate," by the EU Horizon 2020 program (CLOUD-MOTION, Grant 764991), and by the German Federal Ministry of Education and Research (CLOUD-16, Grant 01LK1601C). Open Access funding enabled and organized by Projekt DEAL.

References

Abbatt, J. P. D., Benz, S., Cziczo, D. J., Kanji, Z., Lohmann, U., & Möhler, O. (2006). Solid ammonium sulfate aerosols as ice nuclei: A pathway for cirrus cloud formation. *Science*, *313*(5794), 1770–1773. https://doi.org/10.1126/science.1129726

Adler, G., Koop, T., Haspel, C., Taraniuk, I., Moise, T., Koren, I., et al. (2013). Formation of highly porous aerosol particles by atmospheric freeze-drying in ice clouds. *Proceedings of the National Academy of Sciences of the United States of America*, *110*(51), 20414–20419. https://doi.org/10.1073/pnas.1317209110

Baustian, K. J., Wise, M. E., & Tolbert, M. A. (2010). Depositional ice nucleation on solid ammonium sulfate and glutaric acid particles. *Atmospheric Chemistry and Physics*, *10*(5), 2307–2317. https://doi.org/10.5194/acp-10-2307-2010

Beer, C. G., Hendricks, J., & Righi, M. (2022). A global climatology of ice-nucleating particles under cirrus conditions derived from model simulations with MADE3 in EMAC. *Atmospheric Chemistry and Physics*, *22*(24), 15887–15907. https://doi.org/10.5194/acp-22-15887-2022

Bertozzi, B. (2021). Ice nucleation ability of secondary aerosol particles at cirrus cloud conditions (PhD). Karlsruhe Institute of Technology. https://doi.org/10.5445/IR/1000146739

Bertozzi, B., Wagner, R., Höhler, K., Saathoff, H., Möhler, O., & Leisner, T. (2023). Data sets for the research article "Influence of the neutralization degree on the ice nucleation ability of ammoniated sulfate particles" by Bertozzi, et al. (2024) in the Journal of Geophysical Research (Atmospheres) [Dataset]. Karlsruhe Institute of Technology. https://doi.org/10.35097/1847

Bertozzi, B., Wagner, R., Song, J., Höhler, K., Pfeifer, J., Saathoff, H., et al. (2021). Ice nucleation ability of ammonium sulfate aerosol particles internally mixed with secondary organics. *Atmospheric Chemistry and Physics*, *21*(13), 10779–10798. https://doi.org/10.5194/acp-21-10779-2021

Bhattacharjee, P. S., Sud, Y. C., Liu, X., Walker, G. K., Yang, R., & Wang, J. (2010). Importance of including ammonium sulfate ($(NH_4)_2SO_4$) aerosols for ice cloud parameterization in GCMs. *Annales Geophysicae*, *28*(2), 621–631. https://doi.org/10.5194/angeo-28-621-2010

Bodsworth, A., Zobrist, B., & Bertram, A. K. (2010). Inhibition of efflorescence in mixed organic-inorganic particles at temperatures less than 250 K. *Physical Chemistry Chemical Physics*, *12*(45), 12259–12266. https://doi.org/10.1039/C0CP00572J

Braban, C. F., Abbatt, J. P. D., & Cziczo, D. J. (2001). Deliquescence of ammonium sulfate particles at sub-eutectic temperatures. *Geophysical Research Letters*, *28*(20), 3879–3882. https://doi.org/10.1029/2001gl013175

Chen, Y., DeMott, P. J., Kreidenweis, S. M., Rogers, D. C., & Sherman, D. E. (2000). Ice formation by sulfate and sulfuric acid aerosol particles under upper-tropospheric conditions. *Journal of the Atmospheric Sciences*, *57*(22), 3752–3766. https://doi.org/10.1175/1520-0469(2000)057%3C3752:IFBSAS%3E2.0.CO;2

Clegg, S. L., Brimblecombe, P., & Wexler, A. S. (1998). Thermodynamic model of the system H^+-NH_4^+-SO_4^{2-}-NO_3^--H_2O at tropospheric temperatures. *Journal of Physical Chemistry A*, *102*(12), 2137–2154. https://doi.org/10.1021/jp973042r

Colberg, C. A., Krieger, U. K., & Peter, T. (2004). Morphological investigations of single levitated $H_2SO_4/NH_3/H_2O$ aerosol particles during deliquescence/efflorescence experiments. *Journal of Physical Chemistry A*, *108*(14), 2700–2709. https://doi.org/10.1021/Jp037628r

Colberg, C. A., Luo, B. P., Wernli, H., Koop, T., & Peter, T. (2003). A novel model to predict the physical state of atmospheric $H_2SO_4/NH_3/H_2O$ aerosol particles. *Atmospheric Chemistry and Physics*, *3*(4), 909–924. https://doi.org/10.5194/acp-3-909-2003

Connolly, P. J., Möhler, O., Field, P. R., Saathoff, H., Burgess, R., Choularton, T., & Gallagher, M. (2009). Studies of heterogeneous freezing by three different desert dust samples. *Atmospheric Chemistry and Physics*, *9*(8), 2805–2824. https://doi.org/10.5194/acp-9-2805-2009

Cziczo, D. J., & Abbatt, J. P. D. (2000). Infrared observations of the response of NaCl, $MgCl_2$, NH_4HSO_4, and NH_4NO_3 aerosols to changes in relative humidity from 298 to 238 K. *Journal of Physical Chemistry A*, *104*(10), 2038–2047. https://doi.org/10.1021/jp9931408

Cziczo, D. J., & Abbatt, J. P. D. (2001). Ice nucleation in NH_4HSO_4, NH_4NO_3, and H_2SO_4 aqueous particles: Implications for cirrus cloud formation. *Geophysical Research Letters*, *28*(6), 963–966. https://doi.org/10.1029/2000GL012568

Davis, R. D., Lance, S., Gordon, J. A., Ushijima, S. B., & Tolbert, M. A. (2015). Contact efflorescence as a pathway for crystallization of atmospherically relevant particles. *Proceedings of the National Academy of Sciences of the United States of America*, *112*(52), 15815–15820. https://doi.org/10.1073/pnas.1522860113

DeMott, P. J., Möhler, O., Cziczo, D. J., Hiranuma, N., Petters, M. D., Petters, S. S., et al. (2018). The fifth international workshop on ice nucleation phase 2 (FIN-02): Laboratory intercomparison of ice nucleation measurements. *Atmospheric Measurement Techniques*, *11*(11), 6231–6257. https://doi.org/10.5194/amt-11-6231-2018

Fahey, D. W., Gao, R. S., Möhler, O., Saathoff, H., Schiller, C., Ebert, V., et al. (2014). The AquaVIT-1 intercomparison of atmospheric water vapor measurement techniques. *Atmospheric Measurement Techniques*, *7*(9), 3177–3213. https://doi.org/10.5194/amtd-7-3159-2014

Froyd, K. D., Murphy, D. M., Sanford, T. J., Thomson, D. S., Wilson, J. C., Pfister, L., & Lait, L. (2009). Aerosol composition of the tropical upper troposphere. *Atmospheric Chemistry and Physics*, *9*(13), 4363–4385. https://doi.org/10.5194/acp-9-4363-2009

Ge, C., Zhu, C. Q., Francisco, J. S., Zeng, X. C., & Wang, J. (2018). A molecular perspective for global modeling of upper atmospheric NH_3 from freezing clouds. *Proceedings of the National Academy of Sciences of the United States of America*, *115*(24), 6147–6152. https://doi.org/10.1073/pnas.1719949115

Han, J. H., & Martin, S. T. (1999). Heterogeneous nucleation of the efflorescence of $(NH_4)_2SO_4$ particles internally mixed with Al_2O_3, TiO_2, and ZrO_2. *Journal of Geophysical Research*, *104*(D3), 3543–3553. https://doi.org/10.1029/1998JD100072

Hoose, C., & Möhler, O. (2012). Heterogeneous ice nucleation on atmospheric aerosols: A review of results from laboratory experiments. *Atmospheric Chemistry and Physics*, *12*(20), 9817–9854. https://doi.org/10.5194/acp-12-9817-2012

Jensen, E. J., Kärcher, B., Ueyama, R., Pfister, L., Bui, T. V., Diskin, G. S., et al. (2018). Heterogeneous ice nucleation in the tropical tropopause layer. *Journal of Geophysical Research: Atmospheres*, *123*(21), 12210–12227. https://doi.org/10.1029/2018JD028949

Kärcher, B., DeMott, P. J., Jensen, E. J., & Harrington, J. Y. (2022). Studies on the competition between homogeneous and heterogeneous ice nucleation in cirrus formation. *Journal of Geophysical Research: Atmospheres*, *127*(3), e2021JD035805. https://doi.org/10.1029/2021JD035805

Kirpes, R. M., Lei, Z., Fraund, M., Gunsch, M. J., May, N. W., Barrett, T. E., et al. (2022). Solid organic-coated ammonium sulfate particles at high relative humidity in the summertime Arctic atmosphere. *Proceedings of the National Academy of Sciences of the United States*, *119*(14), e2104496119. https://doi.org/10.1073/pnas.2104496119

Kong, X. R., Wolf, M. J., Roesch, M., Thomson, E. S., Bartels-Rausch, T., Alpert, P. A., et al. (2018). A continuous flow diffusion chamber study of sea salt particles acting as cloud nuclei: Deliquescence and ice nucleation. *Tellus Series B Chemical and Physical Meteorology*, *70*(1), 1463806. https://doi.org/10.1080/16000889.2018.1463806

Koop, T., Bertram, A. K., Molina, L. T., & Molina, M. J. (1999). Phase transitions in aqueous NH_4HSO_4 solutions. *The Journal of Physical Chemistry A*, *103*(45), 9042–9048. https://doi.org/10.1021/jp992033a

Koop, T., Luo, B. P., Tsias, A., & Peter, T. (2000). Water activity as the determinant for homogeneous ice nucleation in aqueous solutions. *Nature*, *406*(6796), 611–614. https://doi.org/10.1038/35020537

Ladino, L. A., Zhou, S., Yakobi-Hancock, J. D., Aljawhary, D., & Abbatt, J. P. D. (2014). Factors controlling the ice nucleating abilities of alpha-pinene SOA particles. *Journal of Geophysical Research: Atmospheres*, *119*(14), 9041–9051. https://doi.org/10.1002/2014jd021578

Liu, L., Mishchenko, M. I., Cairns, B., Carlson, B. E., & Travis, L. D. (2006). Modeling single-scattering properties of small cirrus particles by use of a size-shape distribution of ice spheroids and cylinders. *Journal of Quantitative Spectroscopy and Radiative Transfer*, *101*(3), 488–497. https://doi.org/10.1016/j.jqsrt.2006.02.040

Maloney, C., Toon, B., Bardeen, C., Yu, P., Froyd, K., Kay, J., & Woods, S. (2022). The balance between heterogeneous and homogeneous nucleation of ice clouds using CAM5/CARMA. *Journal of Geophysical Research: Atmospheres*, *127*(6), e2021JD035540. https://doi.org/10.1029/2021JD035540

Marcolli, C. (2014). Deposition nucleation viewed as homogeneous or immersion freezing in pores and cavaties. *Atmospheric Chemistry and Physics*, *14*(4), 2071–2104. https://doi.org/10.5194/acp-14-2071-2014

Martin, S. T., Hung, H. M., Park, R. J., Jacob, D. J., Spurr, R. J. D., Chance, K. V., & Chin, M. (2004). Effects of the physical state of tropospheric ammonium-sulfate-nitrate particles on global aerosol direct radiative forcing. *Atmospheric Chemistry and Physics*, *4*(1), 183–214. https://doi.org/10.5194/acp-4-183-2004

Martin, S. T., Schlenker, J. C., Malinowski, A., Hung, H. M., & Rudich, Y. (2003). Crystallization of atmospheric sulfate-nitrate-ammonium particles. *Geophysical Research Letters*, *30*(21), 2102. https://doi.org/10.1029/2003GL017930

Martinsson, B. G., Friberg, J., Sandvik, O. S., Hermann, M., van Velthoven, P. F. J., & Zahn, A. (2019). Formation and composition of the UTLS aerosol. *npj Climate and Atmospheric Science*, *2*(1), 40. https://doi.org/10.1038/s41612-019-0097-1

Mifflin, A. L., Smith, M. L., & Martin, S. T. (2009). Morphology hypothesized to influence aerosol particle deliquescence. *Physical Chemistry Chemical Physics*, *11*(43), 10095–10107. https://doi.org/10.1039/B910432A

Murphy, D. M., & Koop, T. (2005). Review of the vapour pressures of ice and supercooled water for atmospheric applications. *Quarterly Journal of the Royal Meteorological Society*, *131*(608), 1539–1565. https://doi.org/10.1256/qj.04.94

Nault, B. A., Campuzano-Jost, P., Day, D. A., Jo, D. S., Schroder, J. C., Allen, H. M., et al. (2021). Chemical transport models often underestimate inorganic aerosol acidity in remote regions of the atmosphere. *Communications Earth & Environment*, *2*(1), 93. https://doi.org/10.1038/s43247-021-00164-0

Patnaude, R. J., Perkins, R. J., Kreidenweis, S. M., & DeMott, P. J. (2021). Is ice formation by sea spray particles at cirrus temperatures controlled by crystalline salts? *ACS Earth and Space Chemistry*, *5*(9), 2196–2211. https://doi.org/10.1021/acsearthspacechem.1c00228

Penner, J. E., Zhou, C., Garnier, A., & Mitchell, D. L. (2018). Anthropogenic aerosol indirect effects in cirrus clouds. *Journal of Geophysical Research: Atmospheres*, *123*(20), 11652–11677. https://doi.org/10.1029/2018JD029204

Rogers, D. C. (1988). Development of a continuous flow thermal gradient diffusion chamber for ice nucleation studies. *Atmospheric Research*, *22*(2), 149–181. https://doi.org/10.1016/0169-8095(88)90005-1

Rosenoern, T., Schlenker, J. C., & Martin, S. T. (2008). Hygroscopic growth of multicomponent aerosol particles influenced by several cycles of relative humidity. *The Journal of Physical Chemistry A*, *112*(11), 2378–2385. https://doi.org/10.1021/jp0771825

Schiebel, T. (2017). Ice nucleation activity of soil dust aerosols (PhD). Karlsruhe Institute of Technology. https://doi.org/10.5445/IR/1000076327

Schill, G. P., De Haan, D. O., & Tolbert, M. A. (2014). Heterogeneous ice nucleation on simulated secondary organic aerosol. *Environmental Science and Technology*, *48*(3), 1675–1682. https://doi.org/10.1021/es4046428

Schill, G. P., & Tolbert, M. A. (2013). Heterogeneous ice nucleation on phase-separated organic-sulfate particles: Effect of liquid vs. glassy coatings. *Atmospheric Chemistry and Physics*, *13*(9), 4681–4695. https://doi.org/10.5194/acp-13-4681-2013

Schill, G. P., & Tolbert, M. A. (2014). Heterogeneous ice nucleation on simulated sea-spray aerosol using Raman microscopy. *Journal of Physical Chemistry C*, *118*(50), 29234–29241. https://doi.org/10.1021/jp505379j

Schlenker, J. C., Malinowski, A., Martin, S. T., Hung, H. M., & Rudich, Y. (2004). Crystals formed at 293 K by aqueous sulfate-nitrate-ammonium-proton aerosol particles. *Journal of Physical Chemistry A*, *108*(43), 9375–9383. https://doi.org/10.1021/jp047836z

Schlenker, J. C., & Martin, S. T. (2005). Crystallization pathways of sulfate-nitrate-ammonium aerosol particles. *Journal of Physical Chemistry A*, *109*(44), 9980–9985. https://doi.org/10.1021/jp052973x

Schnaiter, M., Büttner, S., Möhler, O., Skrotzki, J., Vragel, M., & Wagner, R. (2012). Influence of particle size and shape on the backscattering linear depolarisation ratio of small ice crystals—Cloud chamber measurements in the context of contrail and cirrus microphysics. *Atmospheric Chemistry and Physics*, *12*(21), 10465–10484. https://doi.org/10.5194/acp-12-10465-2012

Schneider, J., Höhler, K., Wagner, R., Saathoff, H., Schnaiter, M., Schorr, T., et al. (2021). High homogeneous freezing onsets of sulfuric acid aerosol at cirrus temperatures. *Atmospheric Chemistry and Physics*, *21*(18), 14403–14425. https://doi.org/10.5194/acp-21-14403-2021

Shilling, J. E., Fortin, T. J., & Tolbert, M. A. (2006). Depositional ice nucleation on crystalline organic and inorganic solids. *Journal of Geophysical Research*, *111*(D12), D12204. https://doi.org/10.1029/2005JD006664

Spann, J. F., & Richardson, C. B. (1985). Measurement of the water cycle in mixed ammonium acid sulfate particles. *Atmospheric Environment*, *19*(5), 819–825. https://doi.org/10.1016/0004-6981(85)90072-1

Tabazadeh, A., & Toon, O. B. (1998). The role of ammoniated aerosols in cirrus cloud nucleation. *Geophysical Research Letters*, *25*(9), 1379–1382. https://doi.org/10.1029/97GL03585

Tang, I. N., & Munkelwitz, H. R. (1994). Water activities, densities, and refractive indices of aqueous sulfates and sodium nitrate droplets of atmospheric importance. *Journal of Geophysical Research*, *99*(D9), 18801–18808. https://doi.org/10.1029/94JD01345

Ullrich, R., Hoose, C., Möhler, O., Niemand, M., Wagner, R., Höhler, K., et al. (2017). A new ice nucleation active site parameterization for desert dust and soot. *Journal of the Atmospheric Sciences*, *74*(3), 699–717. https://doi.org/10.1175/JAS-D-16-0074.1

Ushijima, S. B., Davis, R. D., & Tolbert, M. A. (2018). Immersion and contact efflorescence induced by mineral dust particles. *The Journal of Physical Chemistry A*, *122*(5), 1303–1311. https://doi.org/10.1021/acs.jpca.7b12075

Vali, G., DeMott, P. J., Möhler, O., & Whale, T. F. (2015). Technical note: A proposal for ice nucleation terminology. *Atmospheric Chemistry and Physics*, *15*(18), 10263–10270. https://doi.org/10.5194/acp-15-10263-2015

Wagner, R., Benz, S., Möhler, O., Saathoff, H., & Schurath, U. (2006). Probing ice clouds by broadband mid-infrared extinction spectroscopy: Case studies from ice nucleation experiments in the AIDA aerosol and cloud chamber. *Atmospheric Chemistry and Physics*, *6*(12), 4775–4800. https://doi.org/10.5194/acp-6-4775-2006

Wagner, R., Bertozzi, B., Höpfner, M., Höhler, K., Möhler, O., Saathoff, H., & Leisner, T. (2020). Solid ammonium nitrate aerosols as efficient ice nucleating particles at cirrus temperatures. *Journal of Geophysical Research-Atmospheres*, *125*(8), e2019JD032248. https://doi.org/10.1029/2019JD032248

Wagner, R., Kaufmann, J., Möhler, O., Saathoff, H., Schnaiter, M., Ullrich, R., & Leisner, T. (2018). Heterogeneous ice nucleation ability of NaCl and sea salt aerosol particles at cirrus temperatures. *Journal of Geophysical Research: Atmospheres*, *123*(5), 2841–2860. https://doi.org/10.1002/2017JD027864

Wagner, R., Möhler, O., Saathoff, H., & Schnaiter, M. (2014). Enhanced high-temperature ice nucleation ability of crystallized aerosol particles after preactivation at low temperature. *Journal of Geophysical Research: Atmospheres*, *119*(13), 8212–8230. https://doi.org/10.1002/2014jd021741

Wang, J., Hoffmann, A. A., Park, R. J., Jacob, D. J., & Martin, S. T. (2008). Global distribution of solid and aqueous sulfate aerosols: Effect of the hysteresis of particle phase transitions. *Journal of Geophysical Research*, *113*(D11), D11206. https://doi.org/10.1029/2007JD009367

Wang, M., Xiao, M., Bertozzi, B., Marie, G., Rörup, B., Schulze, B., et al. (2022). Synergistic HNO_3–H_2SO_4–NH_3 upper tropospheric particle formation. *Nature*, *605*(7910), 483–489. https://doi.org/10.1038/s41586-022-04605-4

Wise, M. E., Baustian, K. J., & Tolbert, M. A. (2009). Laboratory studies of ice formation pathways from ammonium sulfate particles. *Atmospheric Chemistry and Physics*, *9*(5), 1639–1646. https://doi.org/10.5194/acp-9-1639-2009

Wise, M. E., Baustian, K. J., & Tolbert, M. A. (2010). Internally mixed sulfate and organic particles as potential ice nuclei in the tropical tropopause region. *Proceedings of the National Academy of Sciences of the United States of America*, *107*(15), 6693–6698. https://doi.org/10.1073/pnas.0913018107

Xu, Y., Liu, P., Ma, S., Pei, W., Pang, S., & Zhang, Y. (2022). Efflorescence kinetics of aerosols comprising internally-mixed ammonium sulfate and water-soluble organic compounds. *Atmospheric Environment*, *274*, 119007. https://doi.org/10.1016/j.atmosenv.2022.119007

Zuberi, B., Bertram, A. K., Koop, T., Molina, L. T., & Molina, M. J. (2001). Heterogeneous freezing of aqueous particles induced by crystallized $(NH_4)_2SO_4$, ice, and letovicite. *Journal of Physical Chemistry A*, *105*(26), 6458–6464. https://doi.org/10.1021/jp010094e